

Headline Articles

Dioxygen Reactivity of Copper(I) Complexes with Tetradentate Tripodal Ligands Having Aliphatic Nitrogen Donors: Synthesis, Structures, and Properties of Peroxo and Superoxo Complexes

Kazuya Komiyama, Hideki Furutachi, Shigenori Nagatomo,[1] Akifumi Hashimoto, Hideki Hayashi, Shuhei Fujinami, Masatatsu Suzuki,* and Teizo Kitagawa[1]

Department of Chemistry, Faculty of Science, Kanazawa University, Kakuma-machi, Kanazawa 920-1192

[1]Center for Integrative Bioscience, Okazaki National Research Institutes, Myodaiji, Okazaki 444-8585

Received June 12, 2003; E-mail: suzuki@cacheibm.s.kanazawa-u.ac.jp

Oxygenation of copper(I) with tetradentate tripodal ligands (L) comprised of a tris(aminoethyl)amine (tren) skeleton having sterically bulky substituent(s) on the terminal nitrogens has been investigated, where L = tris(*N*-benzylaminoethyl)amine ($L^{H,Bn}$), tris(*N*-benzyl-*N*-methylaminoethyl)amine ($L^{Me,Bn}$), or tris(*N*,*N*-dimethylaminoethyl)amine ($L^{Me,Me}$). All the copper(I) complexes reacted with dioxygen at low temperatures to produce superoxocopper(II) and/or *trans*-(μ-1,2-peroxo)-dicopper(II) complexes depending on the steric bulkiness of the terminal nitrogens and the reaction conditions. The reaction of a copper(I) complex $[Cu(L^{H,Bn})]^+$ at -90 °C in acetone resulted in the formation of a superoxo complex $[Cu(L^{H,Bn})(O_2)]^+$ as a less stable species and a peroxo complex $[\{Cu(L^{H,Bn})\}_2(O_2)]^{2+}$ as a stable species. The structures of $[Cu(L^{H,Bn})]ClO_4$ and $[\{Cu(L^{H,Bn})\}_2(O_2)](BPh_4)_2 \cdot 8(CH_3)_2CO$ were determined by X-ray crystallography. $[\{Cu(L^{H,Bn})\}_2(O_2)]^{2+}$ has a *trans*-(μ-1,2-peroxo)-dicopper(II) core with a trigonal bipyramidal structure. The O–O bond distance is 1.450(5) Å with an intermetallic Cu···Cu separation of 4.476(2) Å. The resonance Raman spectrum of $[\{Cu(L^{H,Bn})\}_2(O_2)]^{2+}$ measured at -90 °C in acetone-d_6 showed a broad ν(O–O) band at 837–834 cm^{-1} (788 cm^{-1} for an ^{18}O labeled sample) and two ν(Cu–O) bands at 556 and 539 cm^{-1}, suggesting the presence of two peroxo species in solution. $[Cu(L^{Me,Bn})]^+$ also produced both superoxo and *trans*-μ-1,2-peroxo species, $[Cu(L^{Me,Bn})(O_2)]^+$ and $[\{Cu(L^{Me,Bn})\}_2(O_2)]^{2+}$. At a lower concentration of $[Cu(L^{Me,Bn})]^+$ ($\sim$0.24 mM) and higher dioxygen concentration ($P(O_2) = \sim$1 atm), the superoxo species is predominantly formed, whereas at a higher concentration of $[Cu(L^{Me,Bn})]^+$ ($\sim$1 mM) and lower dioxygen concentration ($P(O_2) = \sim$0.02 atm) the formation of the peroxo species is observed. The resonance Raman spectrum of $[Cu(L^{Me,Bn})(O_2)]^+$ ($\sim$1 mM) in acetone-d_6 at ~-95 °C exhibited a ν(O–O) band at 1120 cm^{-1} (1059 cm^{-1} for an ^{18}O labeled sample) and that of $[\{Cu(L^{Me,Bn})\}_2(O_2)]^{2+}$ ($\sim$3 mM) in acetone-d_6 at ~-90 °C showed two ν(O–O) bands at 812 and 797 cm^{-1} (767 and 753 cm^{-1} for an ^{18}O labeled sample), respectively. A similar observation was also made for $[\{Cu(L^{Me,Me})\}_2(O_2)]^{2+}$. Relationships between the energies of the LMCT and d–d transitions and those of the ν(O–O) and ν(Cu–O) stretching vibrations and the steric constraints in the Cu(II)–(O_2^{2-})–Cu(II) core are discussed.

Synthetic copper–dioxygen complexes are of great interest as structural and/or functional models for O_2 transport proteins such as hemocyanin and dioxygen activating copper proteins such as tyrosinase, methane monooxygenase, etc. Various types of Cu_n–O_2 complexes have been developed.[1–4] Some of the complexes, such as *trans*-μ-1,2-peroxo-dicopper(II),[5] μ-η^2:η^2-peroxo-dicopper(II),[6,7] μ^4-η^2-peroxo-tetracopper(II),[8] hydrogenperoxocopper(II),[9] (side-on-superoxo)copper(II),[10] and (side-on-peroxo like)copper(III) complex[11] have been structurally characterized. In addition, bend type μ-η^2:η^2-peroxo,[12] terminal binding or unsymmetric bridging peroxo,[13] and μ-1,1-hydrogenperoxo-dicopper(II) complexes[14] have also been proposed. Formation of bis(μ-oxo)dicopper(III) complexes by the O–O bond scission of the peroxo ligand has also been reported.[15] For the superoxo copper(II) complex, an end-on coordination mode is postulated for the complexes having tetradentate tripodal ligands.[16] Thus, the stereochemistry of the copper–dioxygen complexes is highly flexible depending on the stereochemical and/or electronic effects of the ligands. It is therefore interesting to investigate how the stereochemical and electronic features of supporting ligands influence the formation, structure, and reactivity of copper–dioxygen complexes.

Dioxygen reactivity of a wide variety of copper(I) complexes having various tetradentate tripodal ligands has been investigated.[5,17–31] Detailed kinetic and thermodynamic studies of copper(I) complexes of tmpa[32] and analogous tetradentate tripodal ligands revealed the stepwise formation of a superoxo

Published on the web January 13, 2004; DOI 10.1246/bcsj.77.59

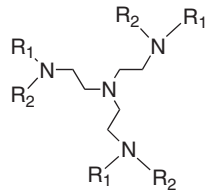

$L^{H,Bn}$: $R_1 = H$, $R_2 = CH_2Ph$
$L^{Me,Bn}$: $R_1 = CH_3$, $R_2 = CH_2Ph$
$L^{Me,Me}$: $R_1 = R_2 = CH_3$

$[Cu^{I}(L)]^{+}$	$[Cu^{II}(L)(O_2)]^{+}$	$[\{Cu^{II}(L)\}_2(O_2)]^{2+}$	$[Cu^{II}(Cl)(L)]^{+}$
($L = L^{H,Bn}$)	($L = L^{H,Bn}$)	($L = L^{H,Bn}$)	($L = L^{H,Bn}$)
($L = L^{Me,Bn}$)	($L = L^{Me,Bn}$)	($L = L^{Me,Bn}$)	($L = L^{Me,Bn}$)
($L = L^{Me,Me}$)	($L = L^{Me,Me}$)	($L = L^{Me,Me}$)	($L = L^{Me,Me}$)

Scheme 1. Tetradentate tripodal ligands and their complexes.

complex $[Cu(tmpa)(O_2)]^{+}$ (Cu:O_2 = 1:1) and a μ-peroxo complex $[\{Cu(tmpa)\}_2(O_2)]^{2+}$ (Cu:O_2 = 2:1).[17] The relative stability of those species has been shown to be dependent on the stereochemical nature of the tripodal ligands. Recently, Schindler et al. have reported similar observations for the copper(I) complexes with $L^{H,Bn}$ and $L^{Me,Me}$ ligands given in Scheme 1. However, the studies are mainly focused on the kinetics of oxygenation of the copper(I) complexes.[24–26] In order to gain further understanding of the properties of copper–dioxygen complexes, structural and spectroscopic studies of copper(I) and the resulting dioxygen-copper(II) complexes are needed.

$$[Cu^{I}(L)]^{+} + O_2 \underset{k_{-1}}{\overset{k_1}{\rightleftharpoons}} [Cu^{II}(L)(O_2)]^{+} \quad (1)$$

$$[Cu^{II}(L)(O_2)]^{+} + [Cu^{I}(L)]^{+} \underset{k_{-2}}{\overset{k_2}{\rightleftharpoons}} [\{Cu^{II}(L)\}_2(O_2)]^{2+} \quad (2)$$

In this study, in order to explore how the nature of the aliphatic nitrogen donors and the alkyl substituents of the supporting ligands derived from a tren framework influences the formation, structure, and properties of copper–dioxygen complexes, we have investigated the oxygenation of a series of Cu(I) complexes with tri- or hexa-alkylsubstituted tren derivatives: $L^{H,Bn}$, $L^{Me,Bn}$, and $L^{Me,Me}$ in Scheme 1, the crystal structure of a *trans*-μ-1,2-peroxo-dicopper(II) complex $[\{Cu(L^{H,Bn})\}_2(O_2)]^{2+}$, and the spectroscopic properties (UV–vis and resonance Raman) of copper–dioxygen complexes. The crystal structures and some physicochemical properties of the copper(II) complexes, $[Cu(Cl)(L)]^{+}$, are also reported.

Experimental

Materials. Acetonitrile and acetone were dried over Molecular Sieves 4A and distilled before use. All other reagents and solvents were commercially available and used without further purification.

Syntheses of Ligands. Tris(*N*-benzylaminoethyl)amine ($L^{H,Bn}$): This was synthesized according to the literature method.[33]

Tris(*N*-benzyl-*N*-methylaminoethyl)amine ($L^{Me,Bn}$): $L^{H,Bn}$ (15.4 g, 37 mmol) was dissolved in formic acid (71.3 g, 1.55 mol), to which 37% formaldehyde (17.34 g, 214 mmol) was added, followed by refluxing for three days at 100 °C. Concentrated hydrochloric acid was added to make the solution acidic (pH = ca. 1), and the mixture was then evaporated to dryness under reduced pressure. The residue was dissolved in water (50 cm^3) and the aqueous solution was washed with three 50 cm^3 portions of diethyl ether. The resulting aqueous solution was made basic (pH ca. 12) by the addition of aqueous NaOH. An oily layer was extracted with three 50 cm^3 portions of chloroform. The chloroform extracts were combined and dried over Na_2SO_4 and filtered. The filtrate was evaporated under a reduced pressure to give a desired ligand as a yellow oil, which was used for preparation of complexes without further purification. Yield: 13.6 g (80%). FAB–MS, $m/z = 456$ $[M - 2]^{+}$. ^1H NMR ($CDCl_3$, 400 MHz) δ 2.14 (9H, s, NCH_3), 2.41 (6H, t, $N(CH_2CH_2N)_3$), 2.62 (6H, t, $N(CH_2CH_2N)_3$), 3.46 (6H, s, NCH_2Ph), 6.82 (15H, m, PhH).

Tris(*N*,*N*-dimethylaminoethyl)amine ($L^{Me,Me}$): This was synthesized according to the literature method.[34]

Synthesis of Complexes. All the manipulations for preparation of the copper(I) complexes were carried out under Ar or N_2 atmosphere using standard Schlenk techniques. (*Caution: All the perchlorate salts are potentially explosive and should be handled with care*).

$[Cu(L^{H,Bn})]ClO_4$: $[Cu(CH_3CN)_4]ClO_4$ (666 mg, 2.04 mmol) was dissolved into an acetone solution (10 cm^3) of $L^{H,Bn}$ (858 mg, 2.06 mmol) under N_2 by warming to afford a colorless solution, to which was added diethyl ether. The resulting solution was allowed to stand for a few hours to give white crystals suitable for X-ray crystallography. Yield: 0.83 g (70%). Anal. Calcd for $C_{27}H_{36}N_4CuClO_4$: C, 55.95; H, 6.26; N, 9.67%. Found: C, 55.87; H, 6.26; N, 9.69%. IR (KBr, cm^{-1}) 1446, 1091 (ClO_4), 748, 698, 623 (ClO_4). ^1H NMR (CD_3COCD_3, 400 MHz, 20 °C) δ 2.83 (6H, t, $N(CH_2CH_2N)_3$), 2.90 (6H, t, $N(CH_2CH_2N)_3$), 3.72 (6H, s, NCH_2Ph), 7.18–7.31 (15H, m, PhH).

$[Cu(L^{H,Bn})]BPh_4$: $[Cu(CH_3CN)_4]ClO_4$ (167 mg, 0.517 mmol) was dissolved into a methanol (10 cm^3)–acetone (2 cm^3) mixture containing $L^{H,Bn}$ (267 mg, 0.640 mmol) under N_2, to which was added a methanol solution (5 cm^3) of $NaBPh_4$ (365 mg, 1.07 mmol). The resulting solution was allowed to stand for a few hours to give white crystals. Yield: 333 mg (80.6%). Calcd for $C_{51}H_{56}N_4BCu$: C, 76.63; H, 7.06; N, 7.01%. Found: C, 76.60; H, 6.94; N 7.06%. IR (KBr, cm^{-1}) 1579 (BPh_4), 1452, 728, 692, 611.

$[Cu(L^{Me,Bn})]ClO_4$: To $L^{Me,Bn}$ (945 mg, 2.06 mmol) in acetone (10 cm^3) was added $[Cu(CH_3CN)_4]ClO_4$ (666 mg, 2.04 mmol) under N_2 to give a pale yellow solution, to which a small amount of diethyl ether was added to produce white crystals. Yield: 1.03 g (81%). Anal. Calcd for $C_{30}H_{42}N_4CuClO_4$: C, 57.96; H, 6.81; N, 9.01%. Found: C, 57.91; H, 6.74; N, 9.26%. IR (KBr, cm^{-1}) 1471, 1455, 1089 (ClO_4), 752, 704, 623 (ClO_4).

$[Cu(L^{Me,Bn})]CF_3SO_3$: This was prepared by the same method for $[Cu(L^{Me,Bn})]ClO_4$ except for using $[Cu(CH_3CN)_4]CF_3SO_3$. Yield: 0.865 g (63%). Calcd for $C_{31}H_{42}N_4CuSO_3F_3$: C, 55.47; H, 6.31; N, 8.35%. Found: C, 55.16; H, 6.25; N, 8.31%. IR (KBr, cm^{-1}) 1471, 1456, 1277 (CF_3SO_3), 1151 (CF_3SO_3), 1030 (CF_3SO_3), 750, 702, 636 (CF_3SO_3). ^1H NMR (CD_3COCD_3, 400 MHz, 20 °C) δ 2.52 (9H, s, NCH_3), 2.94 (6H, t, $N(CH_2CH_2N)_3$), 3.09 (6H, t, $N(CH_2CH_2N)_3$), 3.76 (6H, s, NCH_2Ph), 7.21–7.47 (15H, m, PhH).

$[\{Cu(L^{H,Bn})\}_2(O_2)](BPh_4)_2 \cdot 8(CH_3)_2CO$: Complex $[Cu(L^{H,Bn})]BPh_4$ (100 mg) was dissolved in a small amount of acetone at −78 °C under N_2 and then O_2 gas was introduced into the solution to produce a deep violet color. Diethyl ether was poured gently onto the deep violet solution to make a bilayered solution of diethyl ether and acetone, which was allowed to stand for two days to afford violet crystals suitable for X-ray crystallography.

$[Cu(Cl)(L^{H,Bn})]ClO_4$: To an ethanol solution (20 cm^3) of $L^{H,Bn}$ (458 mg, 1.10 mmol) was added dropwise an ethanol solution (12 cm^3) of $Cu(ClO_4)_2 \cdot 6H_2O$ (370 mg, 1.0 mmol) and LiCl (80 mg, 1.9 mmol) to give a blue powder, which was dissolved

by heating to give a blue solution. The resulting solution was allowed to stand overnight to afford blue crystals suitable for X-ray crystallography. X-ray crystallography of $[Cu(Cl)(L^{H,Bn})]ClO_4$ is given in supplementary materials.[35] Yield: 530 mg (86%). Anal. Calcd for $C_{27}H_{36}N_4CuCl_2O_4$: C, 52.73; H, 5.90; N, 9.11%. Found: C, 52.59; H, 5.98; N, 9.22%. IR (KBr, cm^{-1}) 1454, 1090 (ClO_4), 737, 698, 625 (ClO_4). UV–vis (λ_{max}/nm ($\varepsilon/M^{-1}\,cm^{-1}$ (1 M = 1 mol dm^{-3})) in acetonitrile) 710 (181), 904 (347).

$[Cu(Cl)(L^{H,Bn})]ClO_4\cdot CH_2Cl_2\cdot 0.25H_2O$: The copper(I) complex $[Cu(L^{H,Bn})]ClO_4$ (120 mg, 0.21 mmol) was dissolved in dichloromethane (8 cm^3) under Ar to give a blue-green solution at ambient temperature. After the reaction mixture was stirred for 1 h, a small amount of grayish green powder was precipitated, which was removed by filtration under an air atmosphere and the resulting solution was allowed to stand overnight to give blue crystals suitable for X-ray crystallography. The elemental analysis revealed the loss of CH_2Cl_2 after exposure of the sample under air, although X-ray crystallography showed the above formula (vide infra). Yield: 30 mg (23%). IR and UV–vis spectra were identical to those of $[Cu(Cl)(L^{H,Bn})]ClO_4$ described above. Anal. Calcd for $C_{27}H_{38}CuN_4Cl_2O_5$: C, 51.23; H, 6.05; N, 8.85%. Found: C, 51.35; H, 5.68; N, 8.99%.

$[Cu(Cl)(L^{Me,Bn})]ClO_4\cdot 0.5H_2O$: To an ethanol solution (20 cm^3) of $L^{Me,Bn}$ (505 mg, 1.1 mmol) was added dropwise an ethanol solution (12 cm^3) containing $Cu(ClO_4)_2\cdot 6H_2O$ (370 mg, 1.0 mmol) and LiCl (80 mg, 1.9 mmol) to afford a blue-green solution, from which green crystals were obtained. Recrystallization from a methanol/diethyl ether mixture gave green crystals suitable for X-ray crystallography. Yield: 390 mg (59%). Anal. Calcd for $C_{30}H_{43}N_4CuCl_2O_{4.5}$: C, 54.09; H, 6.51; N, 8.41%. Found: C, 53.75; H, 6.13; N, 8.30%. IR (KBr, cm^{-1}) 1475, 1454, 1092 (ClO_4), 739, 704, 625 (ClO_4). UV–vis (λ_{max}/nm ($\varepsilon/M^{-1}\,cm^{-1}$) in acetonitrile) 744 (289), 934 (705). This complex was also isolated as 2.5 hydrate from $[Cu(L^{Me,Bn})]ClO_4$ in dichloromethane similar to $[Cu(Cl)(L^{H,Bn})]ClO_4\cdot CH_2Cl_2\cdot 0.25H_2O$. Anal. Calcd for $C_{30}H_{47}N_4CuCl_2O_{6.5}$: C, 51.32; H, 6.75; N, 7.98%. Found: C, 51.49; H, 6.65; N, 8.05%. IR and UV–vis spectra were identical to $[Cu(Cl)(L^{Me,Bn})]ClO_4\cdot 0.5H_2O$.

$[Cu(Cl)(tren)]ClO_4$: A methanol solution (5 cm^3) of tren (366 mg, 2.5 mmol) was added dropwise to an aqueous solution (10 cm^3) of $Cu(ClO_4)_2\cdot 6H_2O$ (459 mg, 1.24 mmol) and $CuCl_2\cdot 2H_2O$ (211 mg, 1.24 mmol) to afford blue crystals. Yield: 500 mg (58%). Anal. Calcd for $C_6H_{18}N_4CuCl_2O_4$: C, 20.91; H, 5.26; N, 16.25%. Found: C, 20.90; H, 5.36; N, 16.12%. IR (KBr, cm^{-1}) 1594 (NH_2), 1473, 1089 (ClO_4), 627 (ClO_4). UV–vis (λ_{max}/nm ($\varepsilon/M^{-1}\,cm^{-1}$) in acetonitrile) 740 (187), 932 (440).

$[Cu(L^{Me,Me})]ClO_4$,[24] $[Cu(Cl)(L^{Me,Me})]ClO_4$,[24] $[Cu(tmpa)(CH_3CN)]ClO_4$,[5b] and $[Cu(Cl)(tmpa)]ClO_4$:[36] These were synthesized according to literature methods.

Physical Measurements. Electronic spectra were measured on a Hitachi U-3400 spectrophotometer, and for low temperature measurements, an Otsuka Denshi optical glass fiber attachment with the corrected light path lengths of 1.01 and 0.279 cm was used. Low temperature electronic spectra were also obtained on a Shimadzu MultiSpec-1500 diode array spectrophotometer using a 1 cm or 1 mm quartz cell with a Unisoku thermostated cell holder designed for low-temperature experiments. Infrared spectra were obtained by the KBr-disk method with a HORIBA FT-300B spectrophotometer. ^1H NMR spectra were measured with a JEOL JNM-LA400 spectrometer using tetramethylsilane (TMS) as the internal standard. Cyclic voltammograms were obtained with a BAS CV-27 using a three-electrode configuration, including a glassy carbon working electrode, a platinum coil auxiliary electrode, and a saturated calomel electrode (SCE) as a reference electrode. Acetonitrile was used as the solvent, and *n*-tetrabutylammonium perchlorate as the supporting electrolyte. The $E_{1/2}$ (ΔE) value of ferrocene/ferricinium (Fe^{III}/Fe^{II}) with this set up was 395 mV (92 mV). GC–MS measurements were obtained using a Shimadzu GCMS-QP5050A equipped with a mass spectral detector.

Resonance Raman scattering was measured with a liquid nitrogen cooled CCD detector (Model LN/CCD-1340 × 400PB, Princeton Instruments) attached to a 1 m-single polychromator (Model MC-100DG, Ritsu Oyo Kogaku). The 413.1 nm line of a Kr^+ laser (Model 2060 Spectra Physics), 514.5 nm line of an Ar^+ laser (Model 2017 Spectra Physics), and a dye laser (607 nm) (Model 375B Spectra Physics) with rhodamine-6G dye pumped by an Ar^+ laser were used as the exciting sources. The laser powers used for the 413.1, 514.5, and 607 nm excitations were 9.4, 30, and 50 mW, respectively, at the sample points. All measurements were carried out with a spinning cell (1000 rpm) kept at ~−45 to ~−95 °C. Raman shifts were calibrated with indene and the accuracy of the peak positions of the Raman bands was ±1 cm^{-1}. The spectra of the oxygenated samples of $[Cu(L^{Me,Me})]^+$ were measured by using the samples prepared by mixing stoichiometric amounts of $[Cu(CH_3CN)_4]ClO_4$ and $L^{Me,Me}$ in acetone or acetone-d_6.

X-ray Crystallography. X-ray diffraction studies were made on a Rigaku/MSC Mercury diffractometer and a Rigaku RAXIS-IV imaging plate area detector with graphite monochromated Mo-Kα radiation ($\lambda = 0.71070$ Å (1Å = 1×10^{-10} m)). The structures were solved by direct methods (SHELXS-86 or SIR-92)[37] and expanded using a Fourier technique.[38] The structures were refined by a full-matrix least-squares method by using the teXsan crystallographic software package (Molecular Structure Corporation).[39] Hydrogen atoms were placed at calculated positions. They were included, but not refined, in the final least-squares cycles.

Crystallographic data are summarized in Table 1 and have been deposited at the CCDC, 12 Union Road, Cambridge CB2 1EZ, UK and copies can be obtained on request, free of charge, by quoting the publication citation and deposition numbers CCDC 218701–218705. Experimental details for X-ray crystallography, tables of final atomic coordinates, thermal parameters, and full bond distances and angles are given in the supplementary materials.[35]

$[Cu(L^{H,Bn})]ClO_4$ (I): A single crystal with dimensions of 0.55 × 0.08 × 0.08 mm was picked up on a hand-made cold copper plate mounted inside a liquid N_2 Dewar vessel and mounted on a glass fiber at ca. −80 °C. There are two independent complex cations and two perchlorate anions in an asymmetric unit. All non-hydrogen atoms were refined anisotropically.

$[\{Cu(L^{H,Bn})\}_2(O_2)](BPh_4)_2\cdot 8(CH_3)_2CO$ (II): A dark-violet crystal with dimensions of 0.50 × 0.20 × 0.20 mm was mounted on a glass fiber at ca. −80 °C as described above. The asymmetric unit consists of a half of a complex cation, a tetraphenylborate anion, and four acetone molecules. All non-hydrogen atoms were refined with anisotropic displacement parameters.

$[Cu(Cl)(L^{H,Bn})]ClO_4\cdot CH_2Cl_2\cdot 0.25H_2O$ (III): A block crystal (0.35 × 0.25 × 0.25 mm) was mounted on a glass fiber at ca. −80 °C as described above. The asymmetric unit consists of two independent complex cations and perchlorate anions. The perchlorate anions and dichloromethane molecules were solved by disordered models. All non-hydrogen atoms, except for those of disordered perchlorate anions and dichloromethane molecules, were refined with anisotropic displacement parameters.

Table 1. Crystallographic Data for $[Cu(L^{H,Bn})](ClO_4)$ (**I**), $[\{Cu(L^{H,Bn})\}_2(O_2)](BPh_4)_2\cdot 8(CH_3)_2CO$ (**II**), $[Cu(Cl)(L^{H,Bn})]ClO_4\cdot CH_2Cl_2\cdot 0.25H_2O$ (**III**), and $[Cu(Cl)(L^{Me,Bn})](ClO_4)\cdot 1.5CH_3OH\cdot 0.5H_2O$ (**V**)

	I	**II**	**III**	**V**
Formula	$C_{27}H_{36}N_4O_4ClCu$	$C_{126}H_{160}N_8O_{10}B_2Cu_2$	$C_{28}H_{38.5}N_4O_{4.25}Cl_4Cu$	$C_{31.5}H_{49}N_4O_6Cl_2Cu$
Temp/°C	−150	−116	−116	−150
MW	579.60	2095.41	704.49	714.21
Cryst system	monoclinic	monoclinic	monoclinic	triclinic
Space group	*Pn*	$P2_1/c$	$C2/c$	$P\bar{1}$
a/Å	11.602(1)	15.302(4)	26.652(5)	15.808(1)
b/Å	16.431(1)	18.924(4)	18.226(2)	16.229(2)
c/Å	14.661(2)	21.335(8)	27.444(4)	16.225(1)
α/deg	90	90	90	83.451(7)
β/deg	103.438(6)	108.61(2)	102.20(1)	61.912(4)
γ/deg	90	90	90	79.578(7)
V/Å^3	2718.5(5)	5855(2)	13029(3)	3609.8(5)
Z	4	2	16	4
$2\theta_{max}$	55.0	51.5	51.5	55.0
$F(000)$	1216.0	2240.0	5848.0	1508.0
D_{calcd}/g cm^3	1.416	1.188	1.436	1.314
Abs coeff/cm^{-1}	9.41	4.24	10.38	7.98
No. of reflcns collcd	26297	24879	21187	31465
No. of indpt reflcns	8532 ($I \geq 3\sigma(I)$)	7004 ($I \geq 3\sigma(I)$)	8698 ($I \geq 3\sigma(I)$)	12422 ($I \geq 3\sigma(I)$)
No. of refined params	667	668	736	778
GOF	1.52	1.24	1.66	1.52
Largest peak; hole/e Å^{-3}	1.02; −0.81	1.17; −0.71	1.10; −1.39	1.60; −0.77
R[a)]	0.059	0.058	0.072	0.049
R_w[b)]	0.082	0.087	0.107	0.084

a) $R = \Sigma[|F_o| - |F_c|]/\Sigma|F_o|$. b) $R_w = [\Sigma w(|F_o| - |F_c|)^2/\Sigma w|F_o|^2]^{1/2}$; $w = 1/[\sigma^2(F_o) + p^2|F_o|^2/4]$ ($p = 0.073$ for **I**; $p = 0.092$ for **II**; $p = 0.096$ for **III**; $p = 0.089$ for **V**).

Table 2. Selected Bond Distances (Å) and Angles (°) of $[Cu(L^{H,Bn})](ClO_4)$ (**I**), $[\{Cu(L^{H,Bn})\}_2(O_2)](BPh_4)_2\cdot 8(CH_3)_2CO$ (**II**), $[Cu(Cl)(L^{H,Bn})]ClO_4\cdot CH_2Cl_2\cdot 0.25H_2O$ (**III**), and $[Cu(Cl)(L^{Me,Bn})](ClO_4)\cdot 1.5CH_3OH\cdot 0.5H_2O$ (**V**)

	I	**II**	**III**	**V**
		Bond Distances (Å)		
Cu1–Cl1 (or O1)		1.868(3)	2.261(2)	2.2193(8)
Cu1–N1	2.235(4)	2.104(4)	2.026(4)	2.029(3)
Cu1–N2	2.064(4)	2.142(3)	2.109(5)	2.183(3)
Cu1–N3	2.084(4)	2.083(3)	2.127(5)	2.165(2)
Cu1–N4	2.050(5)	2.149(3)	2.160(4)	2.193(3)
O1–O1*		1.450(5)		
Cu1–Cu1*		4.476(2)		
Cu2–Cl2			2.247(2)	2.2392(9)
Cu2–N5	2.232(4)		2.046(4)	2.022(3)
Cu2–N6	2.077(5)		2.140(5)	2.185(3)
Cu2–N7	2.081(5)		2.134(5)	2.188(3)
Cu2–N8	2.087(4)		2.110(5)	2.184(3)
		Bond Angles (°)		
Cu1–O1–O1*		111.5(3)		
N2–Cu1–N3	119.0(2)	125.4(1)	122.9(2)	119.14(10)
N2–Cu1–N4	126.8(2)	113.8(1)	118.4(2)	119.03(9)
N3–Cu1–N4	111.4(2)	116.4(1)	115.9(2)	119.40(10)
N6–Cu2–N7	115.5(2)		115.1(2)	120.5(1)
N6–Cu2–N8	123.8(2)		115.8(2)	116.1(1)
N7–Cu2–N8	118.2(2)		125.8(2)	120.8(1)

$[Cu(Cl)(L^{H,Bn})]ClO_4$ (IV): A block crystal (0.80 × 0.10 × 0.10 mm) was picked up on the cold copper plate described above, and mounted on a glass fiber at −80 °C. Data were collected at −120 °C. An asymmetric unit consists of a discrete complex cation and one perchlorate anion. All non-hydrogen atoms were refined anisotropically. The crystal structure of the complex cation is given

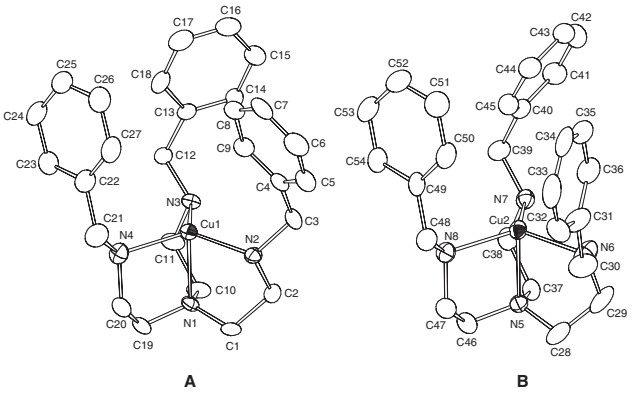

Fig. 1. ORTEP views (50% probability) of two isomers (**A** and **B**) of $[Cu(L^{H,Bn})]ClO_4$ (**I**). Hydrogen atoms are omitted for clarity.

in Fig. S1 in the supplementary materials.[35]

$[Cu(Cl)(L^{Me,Bn})]ClO_4 \cdot 1.5CH_3OH \cdot 0.5H_2O$ (V): A single crystal with dimensions of $0.60 \times 0.50 \times 0.40$ mm was mounted on a glass fiber at ca. -80 °C as described above. There are two independent complex cations and perchlorate anions in an asymmetric unit, respectively. The structures of the two cations are almost mirror images each other. A methanol molecule is present, but disordered. All non-hydrogen atoms of the complex cations and perchlorate anions were refined anisotropically.

Results

The tripodal ligands, $L^{H,Bn}$ and $L^{Me,Bn}$, formed the copper(I) complexes $[Cu(L^{H,Bn})]^+$ and $[Cu(L^{Me,Bn})]^+$, which can be readily isolated as white crystals by the reaction of the corresponding ligand with $[Cu(CH_3CN)_4]^+$ in acetone under N_2. Schindler et al. reported that the isolation of $[Cu(L^{H,Bn})]^+$ was unsuccessful due to serious disproportionation reaction to copper metal and copper(II) complex.[26] However, it was found that a freshly prepared ligand did not cause disproportionation. Use of the ligand under CO_2 gas resulted in serious disproportionation, suggesting that a carbonate salt causes disproportionation. The copper(I) complexes $[Cu(L^{H,Bn})]^+$ and $[Cu(L^{Me,Bn})]^+$ are reactive with dichloromethane. Dissolving the complexes into dichloromethane under Ar at ambient temperature gave blue-green solutions within a few minutes. As mentioned in the experimental section, $[Cu(L^{H,Bn})]^+$ and $[Cu(L^{Me,Bn})]^+$ afforded the corresponding chlorocopper(II) complexes $[Cu(Cl)(L^{H,Bn})]ClO_4 \cdot CH_2Cl_2 \cdot 0.25H_2O$ and $[Cu(Cl)(L^{Me,Bn})]ClO_4 \cdot 2.5H_2O$ from the dichloromethane solution. In addition, GC–MS analysis of a blue-green dichloromethane solution produced by dissolving $[Cu(L^{H,Bn})]^+$ under N_2 atmosphere revealed the formation of 1,2-dichloroethane, which is likely to be derived from the coupling of dichloromethane, as found for the reaction of $[Cu(tmpa)(CH_3CN)]^+$ with organic halides reported by Karlin et al.[40] They also observed that dichloromethane readily reacts with $[Cu(tmpa)(CH_3CN)]^+$ to afford $[Cu(Cl)(tmpa)]^+$ in a high yield. The copper(I) complexes $[Cu(L^{H,Bn})]^+$ and $[Cu(L^{Me,Bn})]^+$ are very reactive with O_2 in solution state, but relatively stable against O_2 in the solid state and can be handled in air.

Structures of $[Cu(L^{H,Bn})]ClO_4$ (I), $[\{Cu(L^{H,Bn})\}_2(O_2)](BPh_4)_2 \cdot 8(CH_3)_2CO$ (II), $[Cu(Cl)(L^{H,Bn})]ClO_4 \cdot CH_2Cl_2 \cdot 0.25H_2O$ (III), and $[Cu(Cl)(L^{Me,Bn})]ClO_4 \cdot 1.5CH_3OH \cdot 0.5H_2O$ (V). X-ray crystallography of $[Cu(L^{H,Bn})]ClO_4$ (**I**) revealed that an asymmetric unit contains two independent molecules (A and B) which are conformational isomers as shown in Fig. 1. The selected bond distances and angles are given in Table 2. The structures of complex cations (A) and (B) are trigonal pyramidal, similar to that of $[Cu(L^{Me,Me})]^+$.[24a] The structural difference in these two isomers is in the orientation of three benzyl groups. The three benzyl groups of molecule (A) have an equatorial orientation with respect to a gauche conformation of the 1,2-diaminoethane chelate ring, whereas one of the benzyl groups in molecule (B) adopts an axial orientation with respect to a gauche conformation of the 1,2-diaminoethane chelate ring and the others an equatorial orientation. The three benzyl groups for both structures form picket fences around the Cu atoms. There is no significant difference in the bond distances and angles around the copper atoms in the two isomers. The average $Cu–N_{eq}$ bond distances of the present type complexes having aliphatic nitrogen donors (2.074 Å for **I** and 2.122 Å for $[Cu(L^{Me,Me})]^+$[24a]) are significantly longer than those of the complexes having aromatic nitrogen donors ($[Cu(tmqa)]^+$ (2.01 and 2.007 Å),[19] $[Cu(Ph_3tren)]^+$ (2.01 Å),[41] $[Cu(Me_2\text{-}tpa)]^+$ (2.008 Å),[15c] $[Cu(Me_3\text{-}tpa)]^+$ (2.01 Å).[42] The long bond distances of **I** and $[Cu(L^{Me,Me})]^+$ are partly due to the steric requirement of the bulky substituents and partly due to the hardness of aliphatic nitrogen donors, which bind more weakly to Cu(I) ion than the aromatic nitrogen donors.

Figure 2 shows the crystal structure of a peroxo complex cation of $[\{Cu(L^{H,Bn})\}_2(O_2)](BPh_4)_2 \cdot 8(CH_3)_2CO$ (**II**), which consists of a centrosymmetric Cu(μ-1,2-O_2)Cu core with $L^{H,Bn}$ ligands. The structure is quite similar to that of $[\{Cu(tmpa)\}_2(O_2)]^{2+}$.[5a] The selected bond distances and angles are given in Table 2. Unlike **I**, the six benzyl groups spread out to accommodate the oxygen atoms of the peroxo ligand and to avoid steric interaction between benzyl groups (Fig. 2a). Each copper ion adopts a five coordinate structure. The structural index parameter ($\tau = (\beta - \alpha)/60$, $\beta > \alpha$) for five-coordinate complexes introduced by Addison et al.[43] is 0.81 comparable to that of $[\{Cu(tmpa)\}_2(O_2)]^{2+}$ ($\tau = 0.86$), where those for an ideal square pyramid and trigonal bipyramid are $\tau = 0$ and $\tau = 1$, respectively. Thus each copper ion has a slightly distorted trigonal bipyramidal structure. The O1–O1* distance is 1.450(5) Å comparable to that of $[\{Cu(tmpa)\}_2(O_2)]^{2+}$ (1.432(6) Å) and those of the peroxo complexes of various transition metal ions.[44] The Cu1–O1 and Cu1–N1 bond distances are 1.868(3) and 2.104(4) Å, respectively, which are also comparable to those of $[\{Cu(tmpa)\}_2(O_2)]^{2+}$ (1.852(5) and 2.104(6) Å, respectively). However, the average $Cu–N_{eq}$ bond distance (2.125 Å) is substantially longer than that of $[\{Cu(tmpa)\}_2(O_2)]^{2+}$ (2.069 Å), which seems to be due to unfavorable steric interaction between the methylene hydrogens of the benzyl groups and the bridging oxygens of the peroxo ligand. The Cu1–O1–O1* angle of 111.5(3)° is slightly larger than that of $[\{Cu(tmpa)\}_2(O_2)]^{2+}$ (107.7(2)°), resulting in slight expansion of the Cu1···Cu1* separation (4.476(2) Å) relative to that of $[\{Cu(tmpa)\}_2(O_2)]^{2+}$ (4.359(1) Å). The space-filling model of **II** shown in Fig. 2b reveals that the Cu(II)(μ-1,2-O_2)Cu(II) core is almost covered by a hydrophobic cavity formed by the six benzyl groups of two

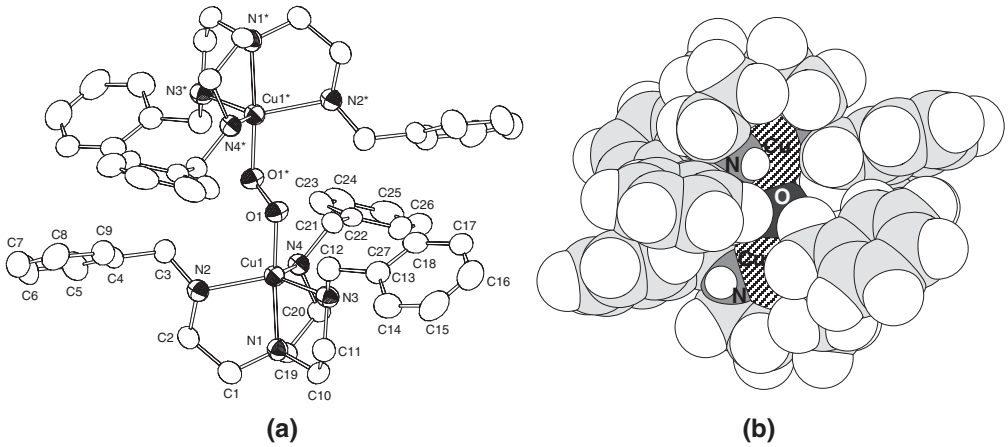

Fig. 2. ORTEP view (50% probability) of the complex cation of $[\{Cu(L^{H,Bn})\}_2(O_2)](BPh_4)_2 \cdot 8(CH_3)_2CO$ (**II**) (**a**) and a space filling view (**b**). Hydrogen atoms are omitted for the ORTEP view.

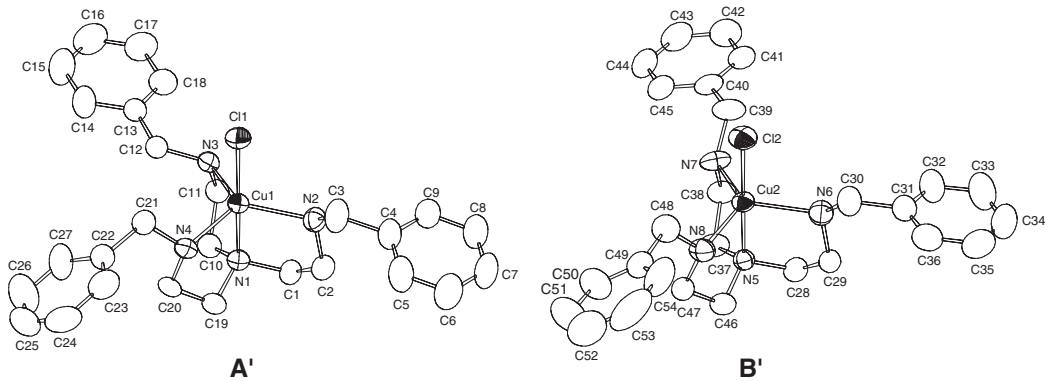

Fig. 3. ORTEP views (50% probability) of complex cations (**A′** and **B′**) of $[Cu(Cl)(L^{H,Bn})]ClO_4 \cdot CH_2Cl_2 \cdot 0.25H_2O$ (**III**). Hydrogen atoms are omitted for clarity.

$L^{H,Bn}$ ligands, which seems to be responsible for protecting the unstable Cu(II)(μ-1,2-O_2)Cu(II) core against some deleterious decay reactions.

X-ray crystallography of the chlorocopper(II) complex $[Cu(Cl)(L^{H,Bn})]ClO_4 \cdot CH_2Cl_2 \cdot 0.25H_2O$ (**III**) showed that an asymmetric unit contains two independent molecules (A′ and B′) which are also the conformational isomers with respect to the orientations of the benzyl groups as found for **I** in Fig. 3. The selected bond distances and angles are given in Table 2. In the course of this study, Schindler reported a crystal structure of a chloride salt ($[Cu(Cl)(L^{H,Bn})]Cl$) which has only one isomer with a symmetric orientation of benzyl groups.[26] The structures of two isomers in **III** are slightly distorted trigonal bipyramidal with the ClN_4 donor set. All the benzyl groups spread out to accommodate a chloride ion as in **II**. There is no significant difference in the metric parameters around the Cu atoms of two isomers. The crystal structure of $[Cu(Cl)(L^{Me,Bn})]ClO_4 \cdot 1.5CH_3OH \cdot 0.5H_2O$ (**V**) also showed that there are two independent complexes in an asymmetric unit. However, they are almost mirror images. One of the complex cations of **V** is given in Fig. 4, and the other one is given in the supplementary materials (Fig. S2).

For the copper(II) complexes, there is a tendency that the average Cu–N_{eq} bond distance becomes longer as the steric bulkiness of the terminal nitrogen donors increases: the average

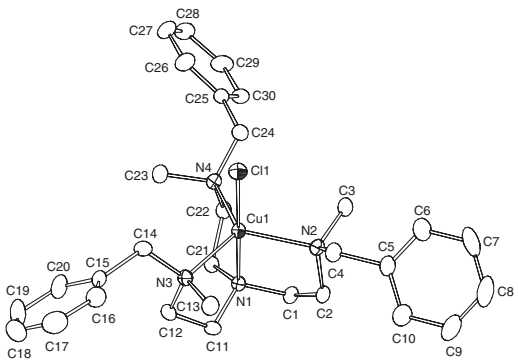

Fig. 4. ORTEP view (50% probability) of one of complex cations of $[Cu(Cl)(L^{Me,Bn})]ClO_4 \cdot 1.5CH_3OH \cdot 0.5H_2O$ (**V**). Hydrogen atoms are omitted for clarity.

Cu–N_{eq} bond distances are 2.06 Å for $[Cu(Cl)(tmpa)]^+$,[36] 2.10 Å for $[Cu(NCS)(tren)]^+$,[45] 2.130 Å for **III**, 2.183 Å for **V**, and 2.186(2) Å for $[Cu(Cl)(L^{Me,Me})]^+$.[24a] Unlike the equatorial bond distances, the Cu–N_{ax} bond distances (2.036 Å for **III** and 2.026 Å for **V**) are comparable to those of $[Cu(Cl)(L^{Me,Me})]^+$ (2.040(6) Å) and $[Cu(Cl)(tmpa)]^+$ (2.050(6) Å), which are significantly shorter than that of **II** (2.104(4) Å).

Electronic Spectra and Electrochemistry. The electronic

Table 3. Electrochemical and Electronic Spectral Data for the Cu(I) and Cu(II) Complexes in Acetonitrile

	$E_{1/2}$ (ΔE_p) mV vs SCE	Spectral data λ_{max}/nm (ε/M^{-1} cm^{-1})	
$[Cu(L^{H,Bn})]^+$	−140 (120)		
$[Cu(L^{Me,Bn})]^+$	+110 (145)		
$[Cu(tmpa)(CH_3CN)]^+$	−10[a] (85)[a]		
$[Cu(Cl)(L^{H,Bn})]^+$	−380 (200)	710 (181),	904 (347)
$[Cu(Cl)(L^{Me,Bn})]^+$	−210 (155)	744 (289),	934 (705)
$[Cu(Cl)(L^{Me,Me})]^+$	−430 (145)	740 (187),	932 (440)[b]
$[Cu(Cl)(tmpa)]^+$	−370[c] (175)	725[sh] (90),	955 (210)[d]
$[Cu(Cl)(tren)]^+$		640[sh] (73),	786 (120)

a) The $E_{1/2}$ value measured in CH_3CN is not reported in Ref. 36b, but −610 mV vs Ag/$AgNO_3$ in DMF is reported. b) The absorption spectrum in CH_3CN is not reported in Ref. 24a, but λ_{max} = 876 nm (ε = 248 M^{-1} cm^{-1}) in water is reported. c) The $E_{1/2}$ value measured in CH_3CN is not reported in Ref. 36b, but −790 mV vs Ag/$AgNO_3$ in DMF is reported. d) Ref. 36b. sh: shoulder.

spectral data of the chlorocopper(II) complexes $[Cu(Cl)(L^{H,Bn})]^+$, $[Cu(Cl)(L^{Me,Bn})]^+$, $[Cu(Cl)(L^{Me,Me})]^+$, $[Cu(Cl)(tmpa)]^+$, and $[Cu(Cl)(tren)]^+$ in acetonitrile are given in Table 3. The electronic spectra of all the chlorocopper(II) complexes exhibit two d–d absorption bands in the 600–1000 nm region, which are characteristic of those of the trigonal bipyramidal copper(II) complexes. A comparison of the absorption maxima of the chloro complexes reveals that the order of the ligand field strength of a series of the tripodal ligands is tren (786 nm) > $L^{H,Bn}$ (904 nm) > $L^{Me,Me}$ (932 nm) ~ $L^{Me,Bn}$ (934 nm) > tmpa (955 nm).[36b] This order indicates that introduction of sterically bulky substituent(s) into the terminal nitrogens of the tren skeleton weakens the ligand field strength and the ligand field strength of pyridyl nitrogens is weaker than that of aliphatic nitrogens. It is noted that there is a tendency that the molar extinction coefficients (ε/M^{-1} cm^{-1}) of $[Cu(Cl)(L^{H,Bn})]^+$, $[Cu(Cl)(L^{Me,Bn})]^+$, and $[Cu(Cl)(L^{Me,Me})]^+$ are significantly larger than those of the other trigonal bipyramidal complexes as seen in Table 3. Especially that of $[Cu(Cl)(L^{Me,Bn})]^+$ is ~700 M^{-1} cm^{-1} at 934 nm, which is exceptionally large for d–d transitions. The origin of such a large molar extinction coefficient, however, is not known at present.

Cyclic voltammograms (CV) of the copper(I) complexes and the chlorocopper(II) complexes measured in acetonitrile showed quasi-reversible waves corresponding to Cu(II)/Cu(I) redox couple. The $E_{1/2}$ values of $[Cu(L^{H,Bn})]^+$ and $[Cu(Cl)(L^{H,Bn})]^+$ are −140 and −380 mV vs SCE, respectively, and those of $[Cu(L^{Me,Bn})]^+$ and $[Cu(Cl)(L^{Me,Bn})]^+$ are +110 and −210 mV vs SCE, respectively (Table 3). Thus, *N*-benzyl-*N*-methylamino groups cause a significant positive shift of $E_{1/2}$ values, indicating that the sterically bulky tertiary amine nitrogen stabilizes the copper(I) oxidation state and/or destabilizes the copper(II) oxidation state compared to the secondary amine nitrogen. These positive shifts of $E_{1/2}$ values for $[Cu(L^{Me,Bn})]^+$ and $[Cu(Cl)(L^{Me,Bn})]^+$ may be partly attributable to the weaker electron donor ability of $L^{Me,Bn}$ relative to that of $L^{H,Bn}$. This is in line with the weaker ligand field strength of the $L^{Me,Bn}$ ligand relative to that of the $L^{H,Bn}$ ligand. It should be noted, however, that the $E_{1/2}$ value of $[Cu(Cl)(L^{Me,Me})]^+$ is −430 mV vs SCE which is significantly negative compared to that of $[Cu(Cl)(L^{Me,Bn})]^+$ (−210 mV vs SCE), even though crystal structural and electronic spectral features of $[Cu(Cl)(L^{Me,Me})]^+$ are quite similar to those of $[Cu(Cl)(L^{Me,Bn})]^+$ as mentioned already. The origin of such a large negative shift for $[Cu(Cl)(L^{Me,Me})]^+$ is not clear at present. The $E_{1/2}$ values of $[Cu(tmpa)(CH_3CN)]^+$ and $[Cu(Cl)(tmpa)]^+$ are −10 and −370 mV vs SCE, respectively, which are between those of $[Cu(L^{H,Bn})]^+$ and $[Cu(L^{Me,Bn})]^+$, and also between those of $[Cu(Cl)(L^{H,Bn})]^+$ and $[Cu(Cl)(L^{Me,Bn})]^+$. Thus, the introduction of benzyl and/or methyl groups on the terminal nitrogens of the tren skeleton has a significant influence on the redox properties of the copper(I) and chlorocopper(II) complexes.

Dioxygen Reactivity of Copper(I) Complexes. Electronic Spectra: The copper(I) complexes $[Cu(L^{H,Bn})]^+$ and $[Cu(L^{Me,Bn})]^+$ in acetone are very reactive toward dioxygen as reported for $[Cu(L^{H,Bn})]^+$ by Schindler et al.[25,26] At room temperature, the complexes underwent instantaneous irreversible oxidation to give the blue copper(II) species, whereas below −80 °C they form dioxygen complexes, which were characterized by X-ray crystallography, electronic, and/or resonance Raman spectroscopy.

Bubbling of O_2 into an acetone solution of $[Cu(L^{H,Bn})]^+$ at −80 °C caused a color change from colorless to deep violet to produce a peroxo species $[\{Cu(L^{H,Bn})\}_2(O_2)]^{2+}$. The electronic spectrum of an acetone solution of $[\{Cu(L^{H,Bn})\}_2(O_2)]^{2+}$ (0.123 mM, all the concentrations for the spectral measurements are given as the copper concentration) at −80 °C exhibits an intense absorption band at 518 nm (ε = 14900 M^{-1} cm^{-1}), two moderately intense bands at ~435 nm (shoulder, ε = ~2800 M^{-1} cm^{-1}) and ~590 nm (ε = ~7700 M^{-1} cm^{-1}), and a weaker band at 976 nm (ε = 300 M^{-1} cm^{-1}, 4.04 mM) as shown in Fig. 5 and Table 4, where the ε values are given based on a dimer $[\{Cu(L^{H,Bn})\}_2(O_2)]^{2+}$. This spectral feature is quite similar to that of $[\{Cu(tmpa)\}_2(O_2)]^{2+}$[5a] as seen in Table 4, indicating that the violet species is a *trans*-(μ-1,2-peroxo)-dicopper(II) complex, $[\{Cu(L^{H,Bn})\}_2(O_2)]^{2+}$, as confirmed by X-ray crystallography. Schindler et al. reported

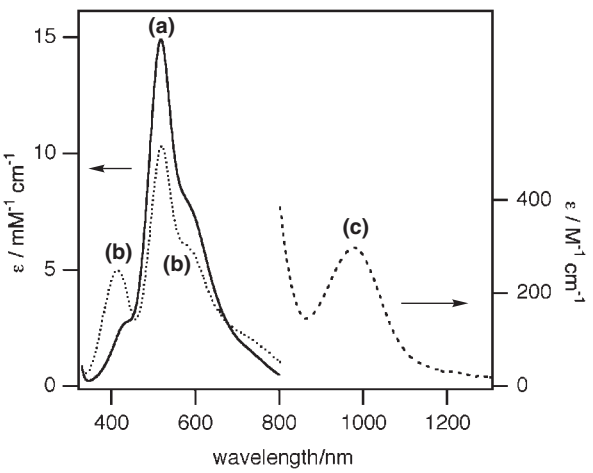

Fig. 5. Electronic spectra of $[Cu(L^{H,Bn})]^+$ in acetone under $P(O_2)$ = ~1 atm; (**a**) at −80 °C (0.123 mM), (**b**) at −90 °C (0.117 mM) and (**c**) at −80 °C (4.04 mM). ε values are given based on a dimer.

Table 4. Spectroscopic Data for Peroxodicopper(II) and Superoxocopper(II) Complexes

Complexes	UV–vis bands λ_{max}/nm (ε/$M^{-1}\,cm^{-1}$)	ν(O–O) ($^{16-18}\Delta$) $\tilde{\nu}$/cm^{-1}	ν(Cu–O) ($^{16-18}\Delta$) $\tilde{\nu}$/cm^{-1}	Ref.
Peroxo complexes				
$[\{Cu(L^{H,Bn})\}_2(O_2)]^{2+}$	~435^{sh} (~2800), 518 (14900), ~590^{sh} (~7700), 976 (300) (d–d band)	839, 829 (51–41)	556 (28), 539 (27)	This work, 26[a]
$[\{Cu(L^{Me,Bn})\}_2(O_2)]^{2+}$	567 (>10000), ~618^{sh} (>8700), ~1088 (>220)	812 (45), 797 (44)	531 (26)	This work
$[\{Cu(L^{Me,Me})\}_2(O_2)]^{2+}$	~460^{sh} (~1500), 553 (~11600), ~615^{sh} (~8600), 1044 (~240)	822 (47), 808 (44^{sh})	535 (25)	This work, 24[b]
$[\{Cu(tmpa)\}_2(O_2)]^{2+}$	~440^{sh} (2000), 525 (11500), ~590^{sh} (7600), 1035 (160)	827 (44)	561 (26)	5, 46, 47
$[\{Cu(^2L)\}_2(O_2)]^{2+}$	565 (17900)	807–746 (753–704)[c]	~550–522 (533–507)[c]	29
$[\{Cu(L^{py})\}_2(O_2)]^{2+}$	550 (10200), 600 (9700)	822 (51)	530 (24)	21a
$[Cu_2(MEPY22PZ)(O_2)]^{2+}$	525 (4010), 625 (2290)	844 (46)	558 (26)	22
$[Cu_2(bpman)(O_2)]^{2+}$	415^{sh} (2333), 505 (10500), 620 (5400)	831 (44)	561	30
$[\{Cu(L^1)\}_2(O_2)]^{2+}$	520, 630	840		23
$[Cu_2(L^2)(O_2)]^{2+}$	495 (7900), 623 (5400)	827		23
Superoxo complexes				
$[Cu(L^{H,Bn})(O_2)]^{+}$	412			This work, 26[d]
$[Cu(L^{Me,Bn})(O_2)]^{+}$	416 (~5400), 591 (~1640), 737 (~2340)	1120 (61)	474 (20)	This work
$[Cu(L^{Me,Me})(O_2)]^{+}$	414	1122		This work, 24[e]
$[Cu(tmpa)(O_2)]^{+}$	410 (4000), 747 (1000)			17, 19
$[Cu(^2L)(O_2)]^{2+}$	416 (4600), 654 (1800)	1120 (62)	450 (8), 422 (5)	29
$[Cu(HB(3\text{-}Ad\text{-}5\text{-}iPrpz)_3)(O_2)]$	383, 452, 699, 980	1043 (59)		10b

sh: shoulder. a) λ_{max} (LMCT) = 506 nm is reported in Ref. 26. b) λ_{max} (LMCT) = 552 nm and ν(O–O) = 825–801 cm^{-1} are reported in Ref. 24b. c) Corresponding relation between the bands may not be clear. d) λ_{max} (LMCT) = 406 nm is reported in Ref. 26. e) λ_{max} (LMCT) = 412 nm (ε = 4800) and ν(O–O) = 1122 cm^{-1} are reported in Ref. 24b.

similar absorption spectra of peroxo and superoxo species (λ_{max} = 506 for peroxo species and λ_{max} = 406 nm for a superoxo species in propionitrile (vide infra)) using time-resolved electronic spectroscopy.[25,26] The intense absorption bands at 518 and ~590 nm can be assigned to the spin-allowed $O_2(\pi_\sigma^*) \rightarrow Cu^{II}(d_{z^2})$ and $O_2(\pi_\nu^*) \rightarrow Cu^{II}(d_{z^2})$ charge transfer (LMCT) transitions, respectively, and the band at ~435 nm to the spin-forbidden $O_2(\pi_\nu^*) \rightarrow Cu^{II}(d_{z^2})$ LMCT transition according to the assignment made for $[\{Cu(tmpa)\}_2(O_2)]^{2+}$ by Solomon et al.[46] The weaker absorption band at 976 nm of $[\{Cu(L^{H,Bn})\}_2(O_2)]^{2+}$ can be attributed to the d–d transitions, which is red-shifted compared to that of the chloro complex $[Cu(Cl)(L^{H,Bn})]^{+}$ (904 nm). Similar observations were made for the peroxo species $[\{Cu(L^{Me,Bn})\}_2(O_2)]^{2+}$, $[\{Cu(L^{Me,Me})\}_2(O_2)]^{2+}$, and $[\{Cu(tmpa)\}_2(O_2)]^{2+}$ relative to the corresponding chloro complexes. Such red shifts of the d–d transitions of the peroxo complexes seem to be partly due to the stronger π donor ability of the coordinated peroxo ligands. $[\{Cu(L^{H,Bn})\}_2(O_2)]^{2+}$ is stable at −80 °C for several hours. Deoxygenation was not effected by bubbling of Ar at −80 °C.

It is noted that the reaction temperature has a significant influence on the oxygenation behavior of $[Cu(L^{H,Bn})]^{+}$. The electronic spectrum of an acetone solution (0.117 mM) at −90 °C under $P(O_2)$ = ~1 atm showed an absorption band at 412 nm together with those of the peroxo species $[\{Cu(L^{H,Bn})\}_2(O_2)]^{2+}$ (Fig. 5b) as already observed by Schindler et al. (λ_{max} = 406 nm at −70 °C in propionitrile) under stopped-flow conditions.[25,26] Under the present reaction conditions, this species is only partially formed. A similar spectrum has already been found upon oxygenation of $[Cu(tmpa)(CH_3CN)]^{+}$, which exhibits a transient absorption band at ~410 nm observable only under stopped-flow conditions.[17] Karlin et al. assigned this transient species to a superoxo species $[Cu(tmpa)(O_2)]^{+}$ (λ_{max} = 410 nm (ε = 4000 $M^{-1}\,cm^{-1}$) and 747 nm (ε = 1000 $M^{-1}\,cm^{-1}$)) and established the stepwise equilibriums given in Eqs. 1 and 2 described above. Bubbling of Ar gas caused the conversion of $[Cu(L^{H,Bn})(O_2)]^{+}$ to $[\{Cu(L^{H,Bn})\}_2(O_2)]^{2+}$, which was completed within a few minutes, indicating that a low dioxygen concentration stabilizes the peroxo species, as can be expected from the stepwise equilibriums Eqs. 1 and 2. The oxygenation is also affected by the concentration of $[Cu(L^{H,Bn})]^{+}$. The electronic spectrum of a more concentrated acetone solution (1.05 mM) at −90 °C under $P(O_2)$ = ~1 atm revealed that the formation of the superoxo species is highly suppressed (not shown in Fig. 5), indicating that higher concentration of $[Cu(L^{H,Bn})]^{+}$ also leads to the formation of the peroxo species as expected from the equilibriums.

The reaction of $[Cu(L^{Me,Bn})]^{+}$ with O_2 in acetone at −90 °C resulted in an immediate color change from pale yellow to green. The electronic spectrum of the green species under these conditions (0.238 mM and $P(O_2)$ = ~1 atm) exhibited three absorption bands at 416 nm (ε = ~5400 $M^{-1}\,cm^{-1}$), ~591 nm (ε = ~1640 $M^{-1}\,cm^{-1}$), and ~737 nm (ε = ~2340 $M^{-1}\,cm^{-1}$) as shown in Fig. 6a, where ε values are given based on a monomer. The formation of a superoxo species $[Cu(L^{Me,Bn})(O_2)]^{+}$ was confirmed by resonance Raman spectrosco-

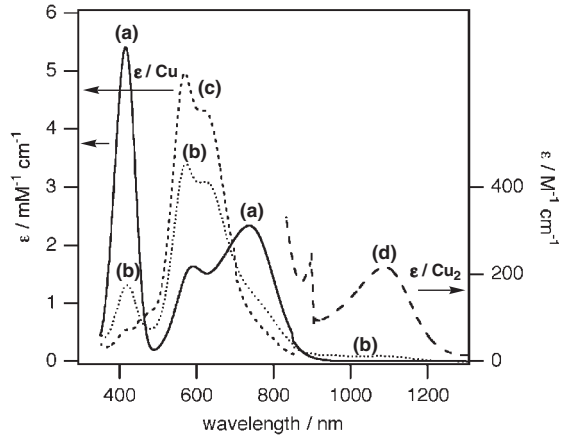

Fig. 6. Electronic spectra of $[Cu(L^{Me,Bn})]^+$ in acetone; (**a**) at −90 °C (0.238 mM and $P(O_2) = \sim 1$ atm), (**b**) at −90 °C after bubbling of Ar gas into the former acetone solution for a few minutes, and (**c**) at −90 °C (1.02 mM and $P(O_2) = \sim 0.02$ atm) measured by an optical fiber with a corrected light path length of 0.279 cm, where ε values for $[\{Cu(L^{Me,Bn})\}_2(O_2)]^{2+}$ should be read as twice as those given in the left hand axis, and (**d**) at −90 °C (1.01 mM and $P(O_2) = \sim 0.02$ atm).

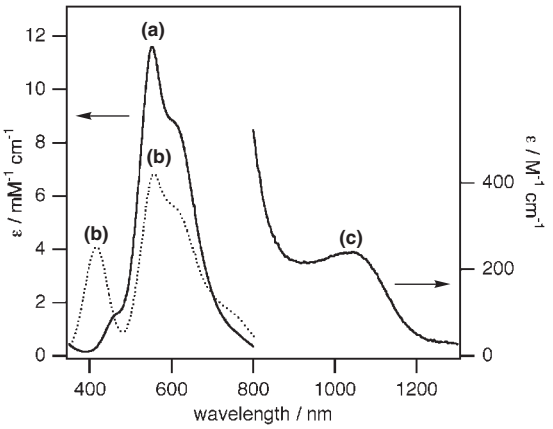

Fig. 7. Electronic spectra of $[Cu(L^{Me,Me})]^+$ in acetone; (**a**) at −90 °C (1.04 mM and $P(O_2) = \sim 0.02$ atm), $[\{Cu(L^{Me,Me})\}_2(O_2)]^{2+}$, (**b**) at −90 °C (0.104 mM and $P(O_2) = \sim 1$ atm), and (**c**) at −90 °C (2.93 mM and $P(O_2) = \sim 0.02$ atm) measured by an optical fiber with a corrected light path length of 0.279 cm. ε values are given based on a dimer.

py (vide infra). There is a possibility that the band at ~591 nm is attributable to an overlapping of the CT band of the peroxo species present as a minor species ($\lambda_{max} = 567$ and 618 nm, vide infra). However, Gaussian analysis revealed that there is no absorption band at 567 or 618 nm. Thus, these three bands are undoubtedly attributable to a superoxo species $[Cu(L^{Me,Bn})(O_2)]^+$. There is no appreciable absorption band up to 1300 nm. Assignment of those absorption bands remains to be made. This superoxo species $[Cu(L^{Me,Bn})(O_2)]^+$ is stable for at least one hour under the conditions. Bubbling of Ar into this solution for a few minutes, however, caused a drastic spectral change. As the 416 nm band decreased, new bands at 567 and 618 nm appeared (Fig. 6b). Although the absorption band at 567 nm is significantly lower in energy than those of $[\{Cu(L^{H,Bn})\}_2(O_2)]^{2+}$ and $[\{Cu(tmpa)\}_2(O_2)]^{2+}$ (518 and 525 nm, respectively), the spectral pattern is characteristic of those of the peroxo species. The formation of a peroxo species was also confirmed by resonance Raman spectroscopy (vide infra). The result clearly indicates that the superoxo species $[Cu(L^{Me,Bn})(O_2)]^+$ can be also converted to a peroxo species $[\{Cu(L^{Me,Bn})\}_2(O_2)]^{2+}$ at low O_2 concentration as observed for $[Cu(L^{H,Bn})(O_2)]^+$. The electronic spectrum of a more concentrated acetone solution (1.02 mM) under $P(O_2) = \sim 0.02$ atm at −90 °C exhibits no appreciable band at 416 nm, but intense bands at 567 ($\varepsilon > 10000\ M^{-1}\,cm^{-1}$), 618 (shoulder, $\varepsilon > 8700\ M^{-1}\,cm^{-1}$), and 1088 nm ($\varepsilon > 220\ M^{-1}\,cm^{-1}$), where the ε values are given based on a dimer, indicating that the peroxo species is solely present under the conditions (Fig. 6c). However, it should be noted that this species decayed within several minutes. Thus, $[\{Cu(L^{Me,Bn})\}_2(O_2)]^{2+}$ is thermally very unstable compared with $[Cu(L^{Me,Bn})(O_2)]^+$ and $[\{Cu(L^{H,Bn})\}_2(O_2)]^{2+}$.

Recently, the electronic spectral changes for successive formation of a superoxo species $[Cu(L^{Me,Me})(O_2)]^+$ and a peroxo species $[\{Cu(L^{Me,Me})\}_2(O_2)]^{2+}$ have been reported by

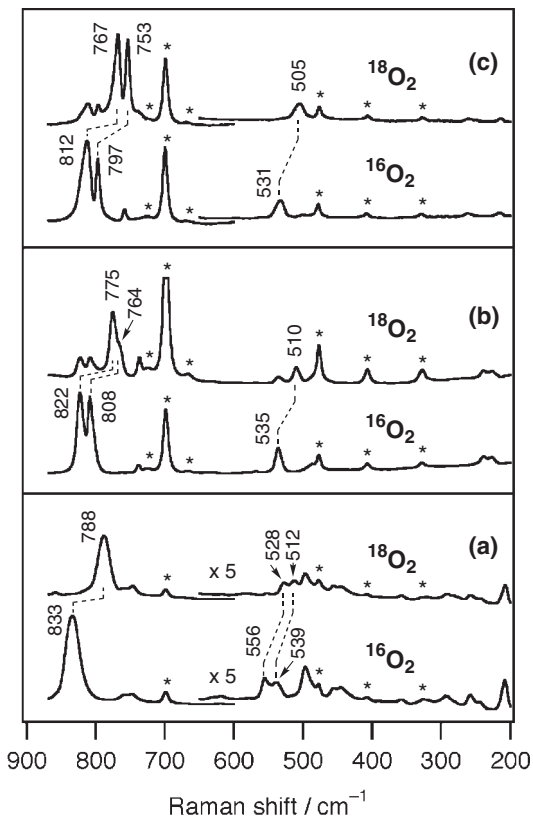

Fig. 8. Resonance Raman spectra of $[\{Cu(L^{H,Bn})\}_2(O_2)]^{2+}$ (**a**) (~7.5 mM) in acetone-d_6 at ~−90 °C with 514.5 nm laser excitation, $[\{Cu(L^{Me,Me})\}_2(O_2)]^{2+}$ (**b**) (~3 mM) in acetone-d_6 at ~−90 °C with 514.5 nm laser excitation, and $[\{Cu(L^{Me,Bn})\}_2(O_2)]^{2+}$ (**c**) (~3 mM) in acetone-d_6 at ~−90 °C with 607 nm laser excitation. The asterisked bands are solvent bands.

Schindler et al.[24] We have also studied the oxygenation behavior of $[Cu(L^{Me,Me})]^+$ depending on changes in temperature, di-

oxygen partial pressure, and concentration of the complex. The spectral behavior is similar to that of $[Cu(L^{Me,Bn})(O_2)]^+$ and $[\{Cu(L^{Me,Bn})\}_2(O_2)]^{2+}$ as shown in Fig. 7. However, unlike the superoxo species of $L^{Me,Bn}$, the superoxo species $[Cu(L^{Me,Me})(O_2)]^+$ is very unstable even under conditions (0.104 mM in acetone at -90 °C under $P(O_2) = \sim 1$ atm), whereas the peroxo species $[\{Cu(L^{Me,Me})\}_2(O_2)]^{2+}$ is stable under conditions (1.04 mM in acetone at -90 °C under $P(O_2) = \sim 0.02$ atm) and no appreciable decay was observed for at least one hour. The electronic spectrum of the peroxo species exhibited the absorption bands (λ_{max}/nm (ε/M^{-1} cm^{-1} based on a dimer); ~460 (shoulder, ~1500), 553 (~11600), 615 (shoulder, ~8600), and 1044 (~240)).

Resonance Raman Spectra: The resonance Raman spectrum of the peroxo species $[\{Cu(L^{H,Bn})\}_2(O_2)]^{2+}$ (~7.5–~1 mM) measured in acetone-d_6 at ~-90 °C with 514.5 nm laser excitation shows isotope-sensitive broad bands at 837–834 (vide infra), 556, and 539 cm^{-1} (788, 528, and 512 cm^{-1} for an ^{18}O labeled sample, respectively) as seen in Fig. 8a and Table 4. The band at 837–834 cm^{-1} can be assigned to the ν(O–O) vibration, and those at 556 and 539 cm^{-1} to the ν(Cu–O) vibrations as found for $[\{Cu(tmpa)\}_2(O_2)]^{2+}$.[46,47] Two ν(Cu–O) vibrations suggest the presence of two peroxo species. The relative intensities of those bands varied with temperature (~-90–~-45 °C) as shown in Fig. 9 and with the concentration of the complex (~7.5–~1 mM) (Fig. S3 in the supplementary materials).[35] The band at 539 cm^{-1} decreases reversibly as the temperature rises and the concentration of the complex decreases. It is also noted that the shape and band position of the ν(O–O) band vary with temperature and concentration: the band shifts from 834 to 837 cm^{-1} with a temperature change from ~-90 to ~-45 °C (~5 mM) as shown in Fig. 9. Gaussian analysis of the bands revealed that the ν(O–O) bands consist of two components which are located at 839 and 829 cm^{-1}.[48] Thus, there is the possibility of the presence of two isomers, although the crystal structure of $[\{Cu(L^{H,Bn})\}_2(O_2)]^{2+}$ showed only one species in the solid state. This temperature and concentration dependency was also observed for the bands at 460–440 cm^{-1} and 760–745 cm^{-1}, although they are not ^{18}O sensitive. There is the possibility that they are conformational isomers as observed in the crystal structures of $[Cu(L^{H,Bn})]^+$ (**I**) and $[Cu(L^{H,Bn})(Cl)]^+$ (**III**). However, it should be noted that the observed spectral changes depending on both temperature and concentration suggest the presence of some complex equilibrium(s) between two species, that may control the relative population of the isomers. Very recently, similar observations have also been found for other complexes having tetradentate tripodal ligand (^2L or $L^{Me,Me}$).[24b,29] For better understanding of this puzzling phenomenon, further study is needed.

The resonance Raman spectrum of the peroxo species $[\{Cu(L^{Me,Bn})\}_2(O_2)]^{2+}$ measured in acetone-d_6 at ~-90 °C with a 607 nm laser excitation showed three isotope-sensitive bands at 812, 797, and 531 cm^{-1} (767, 753, and 505 cm^{-1}

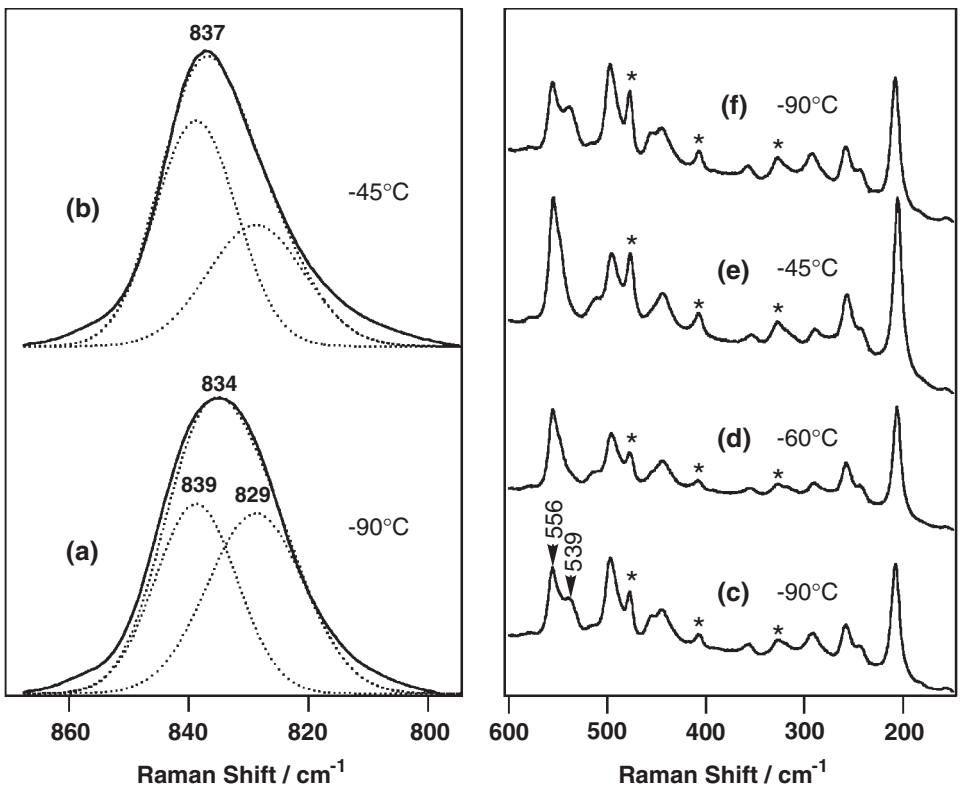

Fig. 9. Temperature dependency of the resonance Raman spectra of the ν(O–O) region of $[\{Cu(L^{H,Bn})\}_2(O_2)]^{2+}$ (~5 mM) in acetone-d_6 at ~-90 °C (**a**) and ~-45 °C (**b**), and that of the ν(Cu–O) region at ~-90 °C (**c**), ~-60 °C (**d**), ~-45 °C (**e**), and ~-90 °C (rechilled) (**f**), where intensities of two ν(O–O) bands (**a** and **b**) are normalized. The ν(O–O) bands were fitted by Gaussian analysis with two peaks at 829 and 839 cm^{-1} constrained to the line widths of 19 and 16 cm^{-1}. The dotted lines are the calculated spectra. The asterisked bands are solvent bands.

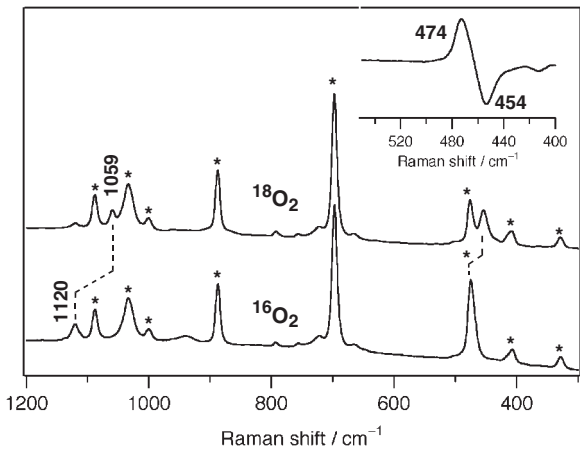

Fig. 10. Resonance Raman spectra of $[Cu(L^{Me,Bn})(O_2)]^+$ with 413.1 nm laser excitation in acetone-d_6 at ~ -95 °C. Inset is a difference spectrum of those of $^{16}O_2$ and $^{18}O_2$ samples. The asterisked bands are solvent bands.

for an ^{18}O labeled sample, respectively) as seen in Fig. 8c. The former two bands are assigned to the ν(O–O) vibrations and the latter to the ν(Cu–O) vibration. There is also the possibility of the presence of two peroxo species similar to $[\{Cu(L^{H,Bn})\}_2(O_2)]^{2+}$, although a splitting due to Fermi-resonance can not be ruled out.

Although recently Schindler et al. reported the Raman spectra of $[\{Cu(L^{Me,Me})\}_2(O_2)]^{2+}$ (data are given Table 4),[24] we also measured the resonance Raman spectra of $[\{Cu(L^{Me,Me})\}_2(O_2)]^{2+}$ in acetone-d_6 at ~ -90 °C. Three isotope sensitive bands were observed at 822, 808, and 535 cm^{-1} (775, shoulder 764, and 510 cm^{-1} for $^{18}O_2$) as seen in Fig. 8b. Relative intensities of the ν(O–O) bands for the $^{16}O_2$ and $^{18}O_2$ samples differ significantly, suggesting that the two ν(O–O) bands are due to Fermi-resonance. However, the origin of two ν(O–O) bands is not clear at present.

The resonance Raman spectrum of the superoxo species $[Cu(L^{Me,Bn})(O_2)]^+$ ($\sim$1 mM) in acetone-d_6 at ~ -95 °C with a 413.1 nm laser excitation showed two isotope-sensitive bands at 1120 and 474 cm^{-1} (1059 and 454 cm^{-1} for an ^{18}O labeled sample) as shown in Fig. 10. The bands at 1120 and 475 cm^{-1} can be assigned to the ν(O–O) and ν(Cu–O) vibrations, respectively. The ν(Cu–O) band at 475 cm^{-1} is significantly lower than those of the peroxo complexes, suggesting a weaker bonding of the superoxo ligand compared to the peroxo ligand. Schindler et al. reported the resonance Raman spectrum of $[Cu(L^{Me,Me})(O_2)]^+$ which exhibited the ν(O–O) at 1122 cm^{-1},[24b] although the spectrum of a $^{18}O_2$ sample was not given. Those ν(O–O) frequencies are characteristic of those of superoxo complexes of various transition metal ions,[44] whereas quite different from that of $[Cu(HB(3\text{-}Ad\text{-}5\text{-}iPrpz)_3)(O_2)]$ (1043 cm^{-1})[10b] in which a superoxide coordinates to the Cu(II) ion as a side-on binding mode.

Discussion

The electrochemistry of the present complexes showed that the introduction of benzyl and/or methyl groups on the terminal nitrogens of the tren skeleton has a significant influence on the redox properties of the copper(I) and chlorocopper(II) complexes. However, dioxygen reactivity of the present copper(I) complexes is mainly dependent on the steric bulkiness of the substituents on the terminal nitrogens, not on the redox properties. It is interesting to explore how the nature of the substituents of the tren derivatives affects the dioxygen reactivity of their copper(I) complexes, and the structures and properties of the resulting copper–dioxygen complexes. Schindler et al. reported that the reaction of $[Cu(tren)]^+$ with O_2 resulted in an instantaneous irreversible oxidation under the same conditions used for the oxygenation of $[Cu(L^{Me,Me})]^+$.[24] However, the introduction of sterically bulky substituents, such as methyl or benzyl group(s), into the terminal nitrogens significantly stabilizes copper–dioxygen complexes, which are observable at low temperatures. The space-filling model of $[\{Cu(L^{H,Bn})\}_2(O_2)]^{2+}$ as shown in Fig. 2b reveals that the Cu(II)(μ-O_2)Cu(II) core is almost completely covered by a hydrophobic cavity formed by the six benzyl groups of $L^{H,Bn}$ ligands, which seems to be responsible for protecting the unstable Cu(II)(μ-O_2)-Cu(II) core against some deleterious decay pathways such as substitution with solvent molecules, a disproportionation reaction between dimers, etc. Such hydrophobic cavities have also been shown to be effective for stabilization of the unstable (μ-peroxo)diiron complexes[49] and high-valent bis(μ-oxo)-dinickel(III) complex.[50] The methyl groups of $L^{Me,Me}$ also have a similar steric effect toward the stabilization of the peroxo species.

As already mentioned, the relative formation ratio of superoxo and peroxo complexes are highly dependent on the concentration of the complex, temperature, and the partial pressure of dioxygen and the steric bulkiness of the substituents on the terminal nitrogens of tren. As expected from the stepwise equilibriums (Eqs. 1 and 2), the superoxo complexes are favored at lower concentrations of the complex and higher dioxygen partial pressure. Complexes $[Cu(L^{H,Bn})]^+$ and $[Cu(L^{Me,Me})]^+$ form both superoxo and peroxo species under the conditions ([complex] = $\sim$0.1 mM, $P(O_2) = \sim$1 atm, and $T = -90$ °C), whereas $[Cu(L^{Me,Bn})]^+$ produces solely a superoxo species under similar conditions. The observed higher stability of the superoxo species $[Cu(L^{Me,Bn})(O_2)]^+$ over the peroxo species $[\{Cu(L^{Me,Bn})\}_2(O_2)]^{2+}$ suggests that steric constraints between the *N*-benzyl-*N*-methyl groups is significant, which prevents dimerization (Eq. 2). The present results show that the steric effect of the *N*-benzyl-*N*-methyl groups is larger than that of the *N*,*N*-dimethyl groups of the $L^{Me,Me}$ ligand for dimerization. It should be noted that $[\{Cu(L^{Me,Bn})\}_2(O_2)]^{2+}$ is thermally unstable compared to the peroxo species of $L^{H,Bn}$ or $L^{Me,Me}$, and readily underwent an irreversible oxidation within several minutes, although the peroxo species of $L^{H,Bn}$ or $L^{Me,Me}$ did not show any appreciable irreversible oxidation for at least one hour under the similar conditions. These results suggest that unfavorable steric interactions between the *N*-benzyl-*N*-methyl groups of the two $L^{Me,Bn}$ ligands prevents not only the formation of a dimer structure but also facilitates irreversible oxidation probably triggered by cleavage of the dimer structure, which overcomes the protection effect of a hydrophobic cavity formed by *N*-benzyl-*N*-methyl groups surrounding the Cu(II)(μ-O_2)-Cu(II) core as observed for $[\{Cu(L^{H,Bn})\}_2(O_2)]^{2+}$.

The steric nature of the terminal nitrogen of the tren derivatives also has a significant influence on the electronic properties

of the peroxo complexes. The spin-allowed $O_2(\pi_\sigma^*) \rightarrow$ Cu(II) LMCT transition energies of the peroxo complexes vary from 518 to 567 nm as seen in Table 4. Karlin et al. suggested that the LMCT transition energy of a *trans*-μ-1,2-peroxo-dicopper(II) complex having a sterically strained structure is lower than that of a complex having a less strained structure.[2,20a] The LMCT and the d–d transition energies roughly reflect the σ bonding strength between the peroxo ligand and copper(II) ion: as the σ bonding of the peroxo ligand becomes stronger, the d_{z^2} orbital energy of copper(II) ion becomes higher, resulting in a higher energy shift of the LMCT and the d–d transitions. The order of the LMCT and the d–d transition energies of the peroxo complexes is $[\{Cu(L^{H,Bn})\}_2(O_2)]^{2+}$ (518 and 976 nm) > $[\{Cu(tmpa)\}_2(O_2)]^{2+}$ (525 and 1035 nm) > $[\{Cu(L^{Me,Me})\}_2(O_2)]^{2+}$ (553 and 1044 nm) > $[\{Cu(L^{Me,Bn})\}_2(O_2)]^{2+}$ (567 and 1088 nm), which seems to reflect the relative degree of steric constraint of the Cu(II)–(O_2^{2-})–Cu(II) cores arising from the steric interactions between the substituents on the terminal nitrogens. The order is not in line with that of the d–d transition energies for the corresponding chloro complexes ($[Cu(L^{H,Bn})(Cl)]^+$ (904 nm) > $[Cu(L^{Me,Bn})(Cl)]^+$ (934 nm) ~ $[Cu(L^{Me,Me})(Cl)]^+$ (932 nm) > $[Cu(tmpa)(Cl)]^+$ (955 nm)) mentioned already, where there is no steric constraint due to ligand–ligand interaction.

The ν(O–O) and ν(Cu–O) frequencies of the present peroxo complexes also vary from 839 to 797 cm^{-1} and from 556 to 531 cm^{-1}, respectively, depending on the steric nature of the terminal nitrogens of the tren derivatives. The order of the ν(O–O) frequencies is $[\{Cu(L^{H,Bn})\}_2(O_2)]^{2+}$ (839 and 829 cm^{-1}) > $[\{Cu(tmpa)\}_2(O_2)]^{2+}$ (827 cm^{-1})[46,47] > $[\{Cu(L^{Me,Me})\}_2(O_2)]^{2+}$ (822 and 808 cm^{-1}) > $[\{Cu(L^{Me,Bn})\}_2(O_2)]^{2+}$ (812 and 797 cm^{-1}) and that of the ν(Cu–O) frequencies is $[\{Cu(tmpa)\}_2(O_2)]^{2+}$ (561 cm^{-1})[46,47] > $[\{Cu(L^{H,Bn})\}_2(O_2)]^{2+}$ (556 and 539 cm^{-1}) > $[\{Cu(L^{Me,Me})\}_2(O_2)]^{2+}$ (535 cm^{-1}) > $[\{Cu(L^{Me,Bn})\}_2(O_2)]^{2+}$ (531 cm^{-1}). There is a rough correlation between the energies of the LMCT and the d–d transitions and those of the ν(O–O) and ν(Cu–O) frequencies as seen in Fig. 11, which includes those of the other *trans*-μ-1,2-peroxo complexes ($\tilde{\nu}$(O–O)/cm^{-1} ($\tilde{\nu}_{max}$/cm^{-1})), 807–746 (17700) for $[\{Cu(^2L)\}_2(O_2)]^{2+}$,[29] 822 (18180) for $[\{Cu(L^{py})\}_2(O_2)]^{2+}$,[21a] 844 (19050) for $[Cu_2(MEPY22PZ)(O_2)]^{2+}$,[22] 831 (19800) for $[Cu_2(bpman)(O_2)]^{2+}$,[30] 840 (19230) for $[\{Cu(L^1)\}_2(O_2)]^{2+}$,[23] and 827 (20200) for $[Cu_2(L^2)(O_2)]^{2+}$.[23] The above tendency may be qualitatively explained in terms of the bonding strength between the peroxo ligand and copper(II) ion: as the interaction increases, the Cu–O bond becomes stronger, and the electron density of the π_σ^* orbital of the peroxo ligand decreases, resulting in an increase of the O–O bond order and the strength of the O–O bond.[14b,47] In order to confirm the above correlations between the LMCT and the d–d transition energies, the ν(O–O) and ν(Cu–O) frequencies, and the thermal stability of the peroxo complexes against irreversible oxidation, further studies are needed.

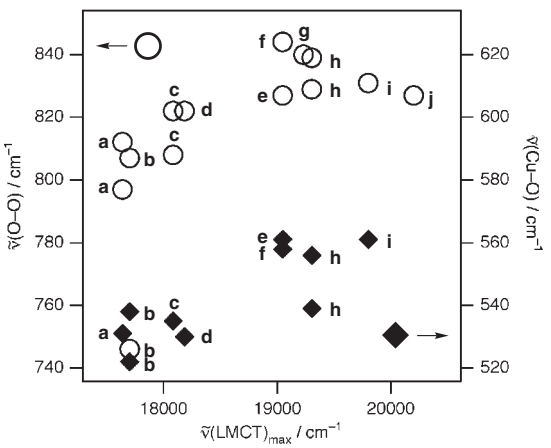

Fig. 11. Correlations between the energies of the spin-allowed $O_2(\pi_\sigma^*) \rightarrow$ Cu(II) LMCT transition and the frequencies of the ν(O–O) (○: left hand axis) and ν(Cu–O) (◆: right hand axis) vibrations of the peroxo complexes. a: $[\{Cu(L^{Me,Bn})\}_2(O_2)]^{2+}$, b: $[\{Cu(^2L)\}_2(O_2)]^{2+}$, c: $[\{Cu(L^{Me,Me})\}_2(O_2)]^{2+}$, d: $[\{Cu(L^{py})\}_2(O_2)]^{2+}$, e: $[\{Cu(tmpa)\}_2(O_2)]^{2+}$, f: $[Cu_2(MEPY22PZ)(O_2)]^{2+}$, g: $[\{Cu(L^1)\}_2(O_2)]^{2+}$, h: $[\{Cu(L^{H,Bn})\}_2(O_2)]^{2+}$, i: $[Cu_2(bpman)(O_2)]^{2+}$, j: $[Cu_2(L^2)(O_2)]^{2+}$.

Formation of a superoxo copper(II) species with a tetradentate tripodal ligand was confirmed by resonance Raman spectroscopy for $[Cu(L^{Me,Bn})(O_2)]^+$, which is thermodynamically stable under the conditions mentioned above. It should be noted that, unlike the peroxo complexes, the superoxo complexes exhibit a relatively intense charge transfer (LMCT) band at 410–420 nm, which shows no remarkable change in the transition energy depending on the coordination environments of the superoxo complexes except for $[Cu(HB(3\text{-}Ad\text{-}5\text{-}iPrpz)_3)(O_2)]$[10b] (see Table 4), which has a bidentate side-on coordination mode. Very recently, Tolman et al. reported that $[Cu(^2L)(O_2)]^+$ also has a side-on coordination mode based on resonance Raman spectra.[29] Unlike $[Cu(HB(3\text{-}Ad\text{-}5\text{-}iPrpz)_3)(O_2)]$, the electronic and Raman spectra of $[Cu(^2L)(O_2)]^+$ (λ_{max}/nm (ε/M^{-1} cm^{-1}) = 416 (4600) and 654 (1800), ν(O–O) = 1120 cm^{-1} ($^{16-18}\Delta$ = 62 cm^{-1})) are quite similar to those of the above superoxo complexes. Although there is no structural information on the superoxo complexes of the present type except for $[Cu(HB(3\text{-}Ad\text{-}5\text{-}iPrpz)_3)(O_2)]$ and $[Cu(^2L)(O_2)]^+$, an end-on terminal coordination mode has been proposed. Thus, further investigations on the relationship between structures and spectroscopic properties are needed.

Summary

The tetradentate tripodal ligand tren can be readily modified stereochemically by introducing various substituent(s) into the terminal nitrogens, which allows to investigate the substituent effect on the properties of copper–dioxygen complexes. The dioxygen reactivity of the copper(I) complexes (dioxygen binding mode and thermal stability of the resulting dioxygen species toward irreversible oxidation) are mainly dependent on the steric bulkiness of the substituents on the terminal nitrogens. Although the redox properties of the copper(I) and copper(II) complexes are also substantially dependent on the substituents, this effect seems to have a minor influence on the dioxygen reactivity of the present copper(I) complexes. The ligands $L^{H,Bn}$ and $L^{Me,Me}$ stabilize the *trans*-(μ-1,2-peroxo)-dicopper(II) species. The crystal structure of the *trans*-(μ-1,2-peroxo)-dicopper(II) complex of $L^{H,Bn}$ showed that the benzyl groups of the $L^{H,Bn}$ ligand form a cavity around the *trans*-(μ-1,2-peroxo)-

dicopper(II) core, which seems to be responsible for protecting the unstable Cu(II)(μ-O_2)Cu(II) core from unfavorable irreversible oxidation. This may be also the case for the observed thermal stability of the peroxo complex $[\{Cu(L^{Me,Me})\}_2(O_2)]^{2+}$, which has *N*,*N*-dimethyl substituents. Thus, a hydrophobic cavity is very effective for stabilizing unstable and reactive species, and probably makes its isolation possible.

The relative formation ratio of the superoxo and peroxo complexes can be controlled by the steric bulkiness of the substituents on the terminal nitrogens and the reaction conditions (concentration of complex, temperature, and dioxygen partial pressure). The *N*-benzyl-*N*-methyl groups of the $L^{Me,Bn}$ ligand greatly suppress the formation of the peroxo species due to significant steric constraints arising from the *N*-benzyl-*N*-methyl groups, and stabilize the superoxo species. Although $[\{Cu(L^{Me,Bn})\}_2(O_2)]^{2+}$ can be generated under the conditions of higher concentration ($\sim$1 mM) and lower dioxygen concentration ($P(O_2) = \sim$0.02 atm) as expected from Eqs. 1 and 2, $[\{Cu(L^{Me,Bn})\}_2(O_2)]^{2+}$ is very unstable and undergoes irreversible oxidation. The results suggest that unfavorable steric interactions between the *N*-benzyl-*N*-methyl groups of the two $L^{Me,Bn}$ ligands suppress not only the formation of a dimer structure, but also facilitates irreversible oxidation.

Significant substituent effects have also been observed for the ν(O–O) and ν(Cu–O) frequencies, and the LMCT and d–d transition energies of the peroxo complexes. The resonance Raman spectroscopy suggests that at least two *trans*-1,2-peroxo species are present in relatively high concentrations at equilibrium. There is a rough correlation between the LMCT and the d–d transition energies and the steric constraint in the Cu(II)(O_2^{2-})Cu(II) core as previously suggested by Karlin et al. In addition, a rough correlation between the ν(O–O), ν(Cu–O), LMCT, and d–d transition energies of the peroxo complex is also observed. This notion seems to be useful in elucidating the steric and/or electronic nature of the Cu(II)(O_2^{2-})Cu(II) core depending on the supporting ligands, although further systematic study is needed.

Financial support of this research by the Ministry of Education, Culture, Sports, Science and Technology Grant-in-Aid for Scientific Research to M. S. and T. K. is gratefully acknowledged.

References

1 N. Kitajima and Y. Moro-oka, *Chem. Rev.*, **94**, 737 (1994).

2 K. D. Karlin, S. Kaderli, and A. D. Zuberbühler, *Acc. Chem. Res.*, **30**, 139 (1997).

3 W. B. Tolman, *Acc. Chem. Res.*, **30**, 227 (1997).

4 K. D. Karlin and A. D. Zuberbühler, "Bioinorganic Catalysis," 2nd ed, revised and expanded, ed by J. Reedijk and E. Bouwman, Marcel Dekker, New York (1999), pp. 469–534.

5 a) R. R. Jacobson, Z. Tyeklár, A. Farooq, K. D. Karlin, S. Liu, and J. Zubieta, *J. Am. Chem. Soc.*, **110**, 3690 (1988). b) Z. Tyeklár, R. R. Jacobson, N. Wei, N. N. Murthy, J. Zubieta, and K. D. Karlin, *J. Am. Chem. Soc.*, **115**, 2677 (1993).

6 a) N. Kitajima, K. Fujisawa, Y. Moro-oka, and K. Toriumi, *J. Am. Chem. Soc.*, **111**, 8975 (1989). b) N. Kitajima, K. Fujisawa, C. Fujimoto, Y. Moro-oka, S. Hashimoto, T. Kitagawa, K. Toriumi, K. Tatsumi, and A. Nakamura, *J. Am. Chem. Soc.*, **114**, 1277 (1992).

7 M. Kodera, K. Katayama, Y. Tachi, K. Kano, S. Hirota, S. Fujinami, and M. Suzuki, *J. Am. Chem. Soc.*, **121**, 11006 (1999).

8 a) J. Reim and B. Krebs, *Angew. Chem., Int. Ed. Engl.*, **33**, 1969 (1994). b) J. Reim, R. Werner, W. Haase, and B. Krebs, *Chem.—Eur. J.*, **4**, 289 (1998).

9 A. Wada, M. Harata, K. Hasegawa, K. Jitsukawa, H. Masuda, M. Mukai, T. Kitagawa, and H. Einaga, *Angew. Chem., Int. Ed.*, **37**, 798 (1998).

10 a) K. Fujisawa, M. Tanaka, Y. Moro-oka, and N. Kitajima, *J. Am. Chem. Soc.*, **116**, 12079 (1994). b) P. Chen, D. E. Root, C. Campochiaro, K. Fujisawa, and E. I. Solomon, *J. Am. Chem. Soc.*, **125**, 466 (2002).

11 N. W. Aboelella, E. A. Lewis, A. M. Reynolds, W. W. Brennessel, C. J. Cramer, and W. B. Tolman, *J. Am. Chem. Soc.*, **124**, 10660 (2002).

12 a) K. D. Karlin, M. S. Haka, R. W. Cruse, G. J. Meyer, A. Farooq, Y. Gultneh, J. C. Hayes, and J. Zubieta, *J. Am. Chem. Soc.*, **110**, 1196 (1988). b) K. D. Karlin, Z. Tyeklár, A. Farooq, M. S. Haka, P. Ghosh, R. W. Cruse, Y. Gultneh, J. C. Hayes, P. J. Toscano, and J. Zubieta, *Inorg. Chem.*, **31**, 1436 (1992). c) E. Pidcock, H. V. Obias, M. Abe, H.-C. Liang, K. D. Karlin, and E. I. Solomon, *J. Am. Chem. Soc.*, **121**, 1299 (1999).

13 a) K. D. Karlin, R. W. Cruse, Y. Gultneh, A. Farooq, J. C. Hayes, and J. Zubieta, *J. Am. Chem. Soc.*, **109**, 2668 (1987). b) J. E. Pate, R. W. Cruse, K. D. Karlin, and E. I. Solomon, *J. Am. Chem. Soc.*, **109**, 2624 (1987).

14 a) K. D. Karlin, P. Ghosh, R. W. Cruse, A. Farooq, Y. Gultneh, R. R. Jacobson, N. J. Blackburn, R. W. Strange, and J. Zubieta, *J. Am. Chem. Soc.*, **110**, 6769 (1988). b) D. E. Root, M. Mahroof-Tahir, K. D. Karlin, and E. I. Solomon, *Inorg. Chem.*, **37**, 4838 (1998).

15 a) J. A. Halfen, S. Mahapatra, E. C. Wilkinson, S. Kaderli, V. G. Young, Jr., L. Que, Jr., A. D. Zuberbühler, and W. B. Tolman, *Science*, **271**, 1397 (1996). b) V. Mahadevan, Z. Hou, A. P. Cole, D. E. Root, T. K. Lal, E. I. Solomon, and T. D. P. Stack, *J. Am. Chem. Soc.*, **119**, 11996 (1997). c) H. Hayashi, S. Fujinami, S. Nagatomo, S. Ogo, M. Suzuki, A. Uehara, Y. Watanabe, and T. Kitagawa, *J. Am. Chem. Soc.*, **122**, 2124 (2000).

16 Crystal structure of a superoxocopper(II) complex has been reported by Harata et al. (M. Harata, K. Jitsukawa, H. Masuda, and H. Einaga, *J. Am. Chem. Soc.*, **116**, 10817 (1994)), but the structure has been claimed by Berreau et al. (L. M. Berreau, S. Mahapatra, J. A. Halfen, V. G. Young, Jr., and W. B. Tolman, *Inorg. Chem.*, **35**, 6339 (1996)).

17 K. D. Karlin, N. Wei, B. Jung, S. Kaderli, P. Niklaus, and A. D. Zuberbühler, *J. Am. Chem. Soc.*, **115**, 9506 (1993).

18 N. Wei, N. N. Murthy, Z. Tyeklár, and K. D. Karlin, *Inorg. Chem.*, **33**, 1177 (1994).

19 N. Wei, N. N. Murthy, Q. Chen, J. Zubieta, and K. D. Karlin, *Inorg. Chem.*, **33**, 1953 (1994).

20 a) D.-H. Lee, N. Wei, N. N. Murthy, Z. Tyeklár, K. D. Karlin, S. Kaderli, B. Jung, and A. D. Zuberbühler, *J. Am. Chem. Soc.*, **117**, 12498 (1995). b) K. D. Karlin, D.-H. Lee, S. Kaderli, and A. D. Zuberbühler, *Chem. Commun.*, **1997**, 475.

21 a) J. A. Halfen, V. G. Young, Jr., and W. B. Tolman, *J. Am. Chem. Soc.*, **118**, 10920 (1996). b) L. M. Berreau, J. A. Halfen, V. G. Young, Jr., and W. B. Tolman, *Inorg. Chim. Acta*, **297**, 115 (2000).

22 J. E. Bol, W. L. Driessen, R. Y. N. Ho, B. Maase, L. Que, Jr., and J. Reedijk, *Angew. Chem., Int. Ed. Engl.*, **36**, 998 (1997).

23 H. Börzel, P. Comba, C. Katsichtis, W. Kiefer, A. Lienke,

V. Nagel, and H. Pritzkow, *Chem.—Eur. J.*, **5**, 1716 (1999).

24 a) M. Becker, F. W. Heinemann, and S. Schindler, *Chem.—Eur. J.*, **5**, 3124 (1999). b) M. Weitzer, S. Schindler, G. Brehm, S. Schneider, E. Hörmann, B. Jung, S. Kaderli, and A. D. Zuberbühler, *Inorg. Chem.*, **42**, 1800 (2003).

25 S. Schindler, *Eur. J. Inorg. Chem.*, **2000**, 2311.

26 M. Schatz, M. Becker, O. Walter, G. Liehr, and S. Schindler, *Inorg. Chim. Acta*, **324**, 173 (2001).

27 M. Schatz, M. Becker, F. Thaler, F. Hampel, S. Schindler, R. R. Jacobson, Z. Tyeklár, N. N. Murthy, P. Ghosh, Q. Chen, J. Zubieta, and K. D. Karlin, *Inorg. Chem.*, **40**, 2312 (2001).

28 M. Weitzer, M. Schatz, F. Hampel, F. W. Heinemann, and S. Schindler, *J. Chem. Soc., Dalton Trans.*, **2002**, 686.

29 B. A. Jazdzewski, A. M. Reynolds, P. L. Holland, V. G. Young, Jr., S. Kaderli, A. D. Zuberbühler, and W. B. Tolman, *J. Biol. Inorg. Chem.*, **8**, 381 (2003).

30 C. He, J. L. DuBois, B. Hedman, K. O. Hodgson, and S. J. Lippard, *Angew. Chem., Int. Ed.*, **40**, 1484 (2001).

31 C. X. Zhang, S. Kaderli, M. Costas, E. Kim, Y.-M. Neuhold, K. D. Karlin, and A. D. Zuberbühler, *Inorg. Chem.*, **42**, 1807 (2003).

32 Abbreviations of ligands used: tmpa = tris(2-pyridylmethyl)amine; tren = tris(aminoethyl)amine; Ph_3tren = tris(4-phenyl-3-aza-3-butenyl)amine; Me_2-tpa = bis(6-methyl-2-pyridylmethyl)(2-pyridylmethyl)amine; Me_3-tpa = tris(6-methyl-2-pyridylmethyl)amine; tmqa = tris(2-quinolylmethyl)amine; MEPY22PZ = [9,22-di(pyridin-2-ylmethyl)-5,13,18,26-tetramethyl-1,4,9,14,17,22,27,28,29,30-decaaza]pentacyclo[22.2.1.1^{4,7}.1^{11,14}.1^{17,20}]triacontan-5,7(28),11(29),12,18,20(30)24(27),25-octaene; L^{py} = 1,4-diisopropyl-7-(2-pyridylmethyl)-1,4,7-triazacyclononane; HB(3-Ad-5-iPrpz)$_3$ = hydrotris(3-adamantyl-5-isopropyl-1-pyrazolyl)-borate; ^{2}L = 1-(2-hydroxy-3,5-di-*tert*-butylbenzyl)-4,7-diisopropyl-1,4,7-triazacyclononane; bpman = 2,7-bis[bis(2-pyridylmethyl)aminomethyl]-1,8-naphthyridine.

33 A. A. Naiini, W. M. P. B. Menge, and J. G. Verkade, *Inorg. Chem.*, **30**, 5009 (1991).

34 M. Ciampolini and N. Nardi, *Inorg. Chem.*, **5**, 41 (1966).

35 Deposited as Document No. 03203 at the Office of the Editor of Bull. Chem. Soc. Jpn.

36 a) K. D. Karlin, J. C. Hayes, S. Juen, J. P. Hutchinson, and J. Zubieta, *Inorg. Chem.*, **21**, 4106 (1982). b) N. Wei, N. N. Murthy, and K. D. Karlin, *Inorg. Chem.*, **33**, 6093 (1994).

37 a) G. M Sheldrick, "SHELXS-86. A Program for Crystal Structure Determination," University of Göttingen, FRG (1986). b) SIR-92: A. Altomare, G. Cascarano, C. Giacovazzo, A. Guagliardi, M. C. Burla, G. Polidori, and M. Camalli, *J. Appl. Crystallogr.*, **27**, 435 (1994).

38 P. T. Beurskens, G. Admiraal, G. Beurskens, W. P. Bosman, R. de Gelder, R. Israel, and J. M. M. Smits, "The DIRDIF-94 program system," Technical Report of the Crystallography Laboratory, University of Nijmegen, The Netherlands (1994).

39 teXsan: Crystal Structure Analysis Package, Molecular Structure Corporation (1985 & 1992).

40 R. R. Jacobson, Z. Tyeklár, and K. D. Karlin, *Inorg. Chim. Acta*, **181**, 111 (1991).

41 E. C. Alyea, G. Ferguson, M. C. Jenning, and Z. Xu, *Polyhedron*, **9**, 739 (1990).

42 H. Hayashi, K. Uozumi, S. Fujinami, S. Nagatomo, K. Shiren, H. Furutachi, M. Suzuki, A. Uehara, and T. Kitagawa, *Chem. Lett.*, **2002**, 416.

43 A. W. Addison, T. N. Rao, J. Reedijk, J. Rijin, and G. C. Verschoor, *J. Chem. Soc., Dalton Trans.*, **1984**, 1349.

44 E. C. Niederhoffer, J. H. Timmons, and A. E. Martell, *Chem. Rev.*, **84**, 137 (1984), and the references therein.

45 P. C. Jain and E. C. Lingafelter, *J. Am. Chem. Soc.*, **89**, 724 (1967).

46 M. J. Baldwin, P. K. Ross, J. E. Pate, Z. Tyeklár, K. D. Karlin, and E. I. Solomon, *J. Am. Chem. Soc.*, **113**, 8671 (1991).

47 M. J. Henson, M. A. Vance, C. X. Zhang, H.-C. Liang, K. D. Karkin, and E. I. Solomon, *J. Am. Chem. Soc.*, **125**, 5186 (2003).

48 The ν(O–O) curves were fitted with two peaks at 829 and 839 cm^{-1} constrained to the line widths of 19 and 16 cm^{-1}.

49 a) Y. Hayashi, T. Kayatani, H. Sugimoto, M. Suzuki, K. Inomata, A. Uehara, Y. Mizutani, T. Kitagawa, and Y. Maeda, *J. Am. Chem. Soc.*, **117**, 11220 (1995). b) T. Ookubo, H. Sugimoto, T. Nagayama, H. Masuda, T. Sato, K. Tanaka, Y. Maeda, H. Okawa, Y. Hayashi, A. Uehara, and M. Suzuki, *J. Am. Chem. Soc.*, **118**, 701 (1996).

50 K. Shiren, S. Ogo, S. Fujinami, H. Hayashi, M. Suzuki, A. Uehara, Y. Watanabe, and Y. Moro-oka, *J. Am. Chem. Soc.*, **122**, 254 (2000).